



Published in final edited form as:

Neuroimage. 2017 August 15; 157: 400–414. doi:10.1016/j.neuroimage.2017.06.003.

Decision ambiguity is mediated by a late positive potential originating from cingulate cortex

Sai Sun¹, Shanshan Zhen^{1,5}, Zhongzheng Fu², Daw-An Wu³, Shinsuke Shimojo³, Ralph Adolphs^{3,4}, Rongjun Yu^{1,5}, Shuo Wang^{4,6}

¹School of Psychology, Center for Studies of Psychological Application, and Key Laboratory of Mental Health and Cognitive Science of Guangdong Province, South China Normal University, Guangzhou, P.R. China, 510631

²Division of Computing and Mathematical Sciences, California Institute of Technology, Pasadena, CA, USA, 91125

³Division of Biology and Biological Engineering, California Institute of Technology, Pasadena, CA, USA, 91125

⁴Humanities and Social Sciences, California Institute of Technology, Pasadena, CA, USA, 91125

⁵Department of Psychology, National University of Singapore, Singapore 117570

⁶Blanchette Rockefeller Neurosciences Institute, West Virginia University, Morgantown, WV 26505, USA

Abstract

People often make decisions in the face of ambiguous information, but it remains unclear how ambiguity is represented in the brain. We used three types of ambiguous stimuli and combined EEG and fMRI to examine the neural representation of perceptual decisions under ambiguity. We identified a late positive potential, the LPP, which differentiated levels of ambiguity, and which was specifically associated with behavioral judgments about choices that were ambiguous, rather than passive perception of ambiguous stimuli. Mediation analyses together with two further control experiments confirmed that the LPP was generated only when decisions are made (not during mere perception of ambiguous stimuli), and only when those decisions involved choices on a dimension that is ambiguous. A further control experiment showed that a stronger LPP arose in the presence of ambiguous stimuli compared to when only unambiguous stimuli were present. Source modeling suggested that the LPP originated from multiple loci in cingulate cortex, a finding we further confirmed using fMRI and fMRI-guided ERP source prediction. Taken together, our findings argue for a role of an LPP originating from cingulate cortex in encoding decisions based on task-relevant perceptual ambiguity, a process that may in turn influence confidence judgment, response conflict, and error correction.

Corresponding authors: Shuo Wang (wangshuo45@gmail.com); Rongjun Yu (psyyr@nus.edu.sg).

Author Contributions

S.Sun, R.A., R.Y., and S.W. designed experiments. S.Sun, S.Z., and S.W. performed research. S.Sun, S.Z., Z.F., D.W., R.Y. and S.W. analyzed data. S.Sun, S.Shimojo, R.A., R.Y., and S.W. wrote the paper. All authors discussed the results and contributed toward the manuscript.

The authors declare no conflict of interest.

Keywords

Late Positive Potential; Perceptual Ambiguity; Face; Decision; Cingulate Cortex

Introduction

We are frequently bombarded by sensory information whose relevance to a behavioral choice is ambiguous, and we often have to make decisions when choice options have uncertain outcomes. A distributed network of brain areas is implicated in decision making under ambiguity and risk (Krain et al., 2006). In particular, the prefrontal cortex, striatum, anterior insula, and amygdala have been implicated in ambiguous monetary gambles (Hsu et al., 2005, Huettel et al., 2006, Levy et al., 2010) and the inferior frontal gyrus (IFG) and posterior parietal cortex are associated with ambiguous outcome anticipation (Bach et al., 2009). In goal-directed navigation and reinforcement learning, medial prefrontal cortex and basal ganglia are involved in resolving ambiguity (Yoshida and Ishii, 2006), whereas lesions of the orbitofrontal cortex impair decisions under ambiguity and risk (Hsu et al., 2005). While many of these studies have focused on value-based decisions, and have separately studied risk and ambiguity, we here investigated perceptual decisions when the mapping of stimulus category to choice was ambiguous.

In the perceptual domain, unpredictability of stimuli, even without any motivational information, activates the amygdala in both mice and humans (Herry et al., 2007). One highly salient stimulus category encountered in everyday life that features pronounced ambiguity are facial expressions of emotions, which are frequently confused with one another (Young et al., 1997). A recent study has shown that single neurons in the human amygdala signal levels of emotion ambiguity (Wang et al., 2017). However, these prior studies leave unclear exactly what is represented in the brain, and at what point in processing ambiguity arises. A larger literature has focused on a scalp-evoked late positive potential (LPP, beginning about 400ms after stimulus onset) that is sensitive to ambiguous facial expressions (Calvo et al., 2013) as well as to racially ambiguous faces (Willadsen-Jensen and Ito, 2006). The LPP is also involved in evaluating socially relevant concepts (Cunningham et al., 2005), processing affective pictures (Cuthbert et al., 2000, Schupp et al., 2000, Leite et al., 2012), and coding stimulus uncertainty (Sutton et al., 1965a). Given the LPP's role in coding faces, emotion, uncertainty, and combinations of these attributes, we here directly tested how the LPP responds to ambiguous emotional faces, and importantly, which specific attribute the LPP encodes. Furthermore, the LPP is not only associated with accumulating sensory information but also determining choices (O'Connell et al., 2012, Kelly and O'Connell, 2013, Murphy et al., 2015), two aspects that we aimed to further tease apart in the present study with a series of control experiments. Finally, we also investigated how the LPP emerges and unfolds in time, providing mechanistic insight of how the LPP encodes perceptual ambiguity.

Source estimation in prior studies has suggested that the LPP arises from a distributed brain network, including the anterior cingulate cortex (ACC), posterior cingulate cortex (PCC), and insula (Liu et al., 2012, Peng et al., 2012, Yoder and Decety, 2014). On the one hand, the

dorsal ACC (dACC) is thought to play a role in cognitive control, including the detection of performance errors and the monitoring of conflict (Cole et al., 2009, Alexander and Brown, 2010, Shackman et al., 2011, Sheth et al., 2012, Shenhav et al., 2013), reward-based decision making and learning more generally (Kennerley et al., 2006), and representation of both social and physical pain (Lieberman and Eisenberger, 2005). On the other hand, the ventral ACC (vACC) is involved in fear extinction (Etkin et al., 2011) and emotion regulation (Etkin et al., 2015). Across many decision-making paradigms and stimulus modalities, greater vACC activation is associated with the choice with greater positive value (Rushworth and Behrens, 2008, Bartra et al., 2013). In particular, vACC activation reflects both value comparison and confidence in the value comparison process (De Martino et al., 2013), even if no explicit confidence judgment is required of the participants (Lebreton et al., 2015). While there are functional segregations within the ACC (see (Shackman et al., 2011, Etkin et al., 2015) for details) and a single unifying principle that might encompass the function of the entire ACC remains elusive, most of the above functions involve the processing of ambiguity in some form. Ambiguity inherently involves conflict in how sensory information maps onto categories or choices, requires continuous monitoring of ongoing actions, triggers dynamic adjustments in cognitive control, and inversely correlates with confidence in judgment. Prior research has shown that ambiguous decision making is associated with activity in both dACC and vACC (Krain et al., 2006). Ambiguous emotional faces relative to unambiguous emotional faces activate the dACC, whereas ambiguous affective decisions relative to ambiguous gender decisions activate the vACC (Simmons et al., 2006). We therefore hypothesized that the ACC is involved in processing faces with ambiguous emotions, and we here used a combination of source localization together with fMRI in order to help further constrain the putative generators of the LPP within the ACC.

In this study, we found that the LPP encodes levels of perceptual ambiguity. In order to characterize the nature of the LPP and elaborate its role in coding ambiguity, we used a combination of EEG and fMRI, and found that the LPP was strongly associated with choices made about ambiguous stimuli, but not mere perception of ambiguous stimuli. This relationship was formally captured by a statistical mediation model, and two additional experiments directly manipulating whether decisions were made, and whether decisions were about ambiguity, confirmed the specificity of the LPP in coding ambiguity. We also found that a stronger LPP emerged in the context of ambiguous stimuli, but diminished in the context of unambiguous stimuli. The LPP was localized to the vACC, PCC, and insula, and fMRI and fMRI-guided ERP source prediction confirmed these regions. Together, our results reveal a neural signature from a specific network of brain regions that encodes the ambiguity with which stimuli can be classified into categorical decisions.

Materials and Methods

Subjects

In the main task (face judgment task with fear-happy morphed emotions), 23 subjects (17 female, mean age and SD, 22.4±2.17 years) participated in the electroencephalogram (EEG) experiment, 19 subjects (15 female, 20.9±2.02 years) participated in the functional magnetic resonance imaging (fMRI) experiment, and 24 subjects (16 female, 22.3±3.39 years)

participated in the behavioral experiment with confidence ratings. Furthermore, 18 subjects (13 female, 19.8 ± 1.20 years) participated in the EEG control experiment with speeded response, 15 subjects (9 female, 20.7 ± 1.61 years) participated in the EEG control experiment of behavioral response, and 32 subjects (15 female, 20.6 ± 1.79 years) participated in the EEG control experiment of ambiguity context. All subjects were unique and involved in only one separated experiment. All subjects provided written informed consent according to protocols approved by the institutional review board of the South China Normal University.

Stimuli and task

In the face judgment task with fear-happy morphed emotions, stimuli were morphed expression continua between exemplars of fearful and happy expressions. Four individuals (two female) were chosen from the STOIC database (Roy et al., 2007), a database of face images expressing highly recognizable emotions. For each individual we selected unambiguous exemplars of fearful and happy expressions as evaluated with normative rating data provided by the database creators. To generate the morphed expression continua for this experiment, we interpolated pixel value and location between fearful exemplar faces and happy exemplar faces using a piece-wise cubic-spline transformation over a Delaunay tessellation of manually selected control points. We created 5 levels of fear-happy morphs, ranging from 30% fear/70% happy to 70% fear/30% happy in steps of 10% (Fig. 1B). Low-level image properties were equalized by the SHINE toolbox (Willenbockel et al., 2010) (The toolbox features functions for specifying the (rotational average of the) Fourier amplitude spectra, for normalizing and scaling mean luminance and contrast, and for exact histogram specification optimized for perceptual visual quality).

In each trial, a face was presented for 1 second followed by a question prompt asking subjects to make the best guess of the facial emotion. Subjects reported faces as fearful or happy by pressing a button on the keyboard (behavioral and EEG subjects) or response box (fMRI subjects) with either their left or right index fingers. After stimulus offset, subjects had 2 seconds to respond, otherwise the trial was aborted and discarded. Subjects were instructed to respond as quickly as possible, but only after stimulus offset. No feedback message was displayed and the order of faces was completely randomized for each subject. An inter-trial-interval (ITI) was jittered randomly with a uniform distribution between 1 to 2 seconds for behavioral and EEG subjects and 2-8 seconds for fMRI subjects. Behavioral subjects performed 252 trials in 3 blocks, EEG subjects performed 252 trials in 2 blocks, and fMRI subjects performed 168 trials in 2 blocks. All trials were pooled for analysis. In each block, there were equal numbers of trials for each morph level and each identity.

Behavioral subjects also performed a confidence rating. After emotion judgment and a 500ms blank screen, subjects were asked to indicate their confidence of judgment, by pushing the button '1' for 'very sure', '2' for 'sure' or '3' for 'unsure'. As with the emotion judgment, subjects had 2 seconds to respond before the trial was aborted, and no feedback message was displayed.

In the speeded version of the task, subjects were instructed to respond as quickly as possible. The stimulus stayed on the screen until button press. Similarly, subjects had 2 seconds to

respond, otherwise the trial was aborted and discarded. In contrast to the main task, the question prompt asking subjects to make the best guess of the facial emotion preceded the stimulus and was presented for 500ms. Subjects performed 280 trials in 2 blocks.

We performed three control EEG tasks, two for behavioral response (Control Experiment 1-2) and one for ambiguity context (Control Experiment 3). In Control Experiment 1 (168 trials in 1 block), subjects freely viewed the fear-happy morphed faces without pressing any buttons. In Control Experiment 2 (252 trials in 2 blocks), subjects were instructed to discriminate whether the stimulus was a human or an animal, using ambiguous anger-disgust morphed faces and cat-dog morphed animals (Fig. 1B). Anger-disgust morphs were created by FaceGen Modeller (<http://facegen.com/>). Similar to fear-happy morphs, we also selected 4 identities (2 males and 2 females from 3D human face models; two Asian (1 male and 1 female) and two Caucasian), with 2 unambiguous faces and 5 morph levels for each identity. The morphs ranged from 30% anger/70% disgust to 70% anger/30% disgust in steps of 10%. Cat-dog morphed stimuli were used and described in detail in a previous study (Freedman et al., 2001). In brief, there were two cat identities and two dog identities. Each cat identity was morphed with another dog identity to create 4 morph lines. Similarly, each morph line had 2 unambiguous animals and 5 ambiguous morph levels (20% cat/80% dog, 40% cat/60% dog, 50% cat/50% dog, 60% cat/40% dog, and 80% cat/20% dog).

Similar to the main task, Control Experiment 3 was also a face judgment task with fear-happy morphed emotions. However, in the first and third block (64 trials each), subjects only judged unambiguous faces, whereas in the second block (192 trials), subjects judged both unambiguous faces and morphed faces (identical to the main task). Note that we also tested two conditions of breaks between blocks: in 16 subjects, there were no breaks between blocks, whereas in the other 16 subjects, there were 2-minute breaks between blocks.

Behavioral data analysis: emotion judgment index (EJI)

We fitted a logistic function to obtain smooth psychometric curves (Fig. 1C):

$$P(x) = \frac{P_{inf}}{1 + e^{-\alpha(x - x_{half})}}$$

where P is the percentage of trials judging faces as fear, x is the morph level, P_{inf} is the value when x approaches infinity (the curve's maximum value), x_{half} is the symmetric inflection point (the curve's midpoint), and α is the steepness of the curve. P_{inf} , x_{half} , and α were fitted from the observed data (P and x). We derived these parameters for each subject.

We defined an emotion judgment index (EJI) as the point (along the x-axis in Fig. 1C) where the percentage of trials judging faces as fear (y-axis) reaches 50%. We derived the EJI from the fitted curve for each subject.

Electroencephalogram (EEG): data recording

Subjects were seated comfortably about 1.1m in front of a computer screen in a dimly lit and electromagnetically shielded room. Experiments were administered on a 19-inch ($37.7 \times$

30.1cm screen size) IBM LCD display (1280 × 1024 screen resolution). Stimuli were presented using E-prime. EEGs were recorded using a digital AC amplifier from 32 scalp sites with tin electrodes mounted in an elastic cap (NeuroScan4.5) according to the International 10-20 system. EEGs were recorded from the following sites: frontal: FP1, FP2, F7, F3, Fz, F4, F8; frontal-central: FC3, FCz, FC4; central: C3, Cz, C4; central-parietal: CP3, CPz, CP4; parietal: P7, P3, Pz, P4, P8; frontal-temporal-parietal: FT7, TP7, T7, T8, TP8, FT8; and occipital: O1, Oz, O2 (Fig. 2A). The vertical-oculograms (VEOG) were recorded from left supra-orbital and infra-orbital electrodes. The horizontal electro-oculograms (HEOG) were measured from electrodes placed lateral to the outer canthi of the left and right eyes. The ground electrode was placed on the forehead. One reference electrode was placed at the left mastoid and the other at the right mastoid, and all recordings were referenced to the right mastoid. All impedance was maintained below 5K Ω . EEG and electro-oculogram (EOG) were amplified using a 0.05-70Hz band-pass filter and were continuously sampled at 500Hz/channel.

EEG: data preprocessing

EEG data were processed using EEGLAB (Delorme and Makeig, 2004), an open source toolbox running in the MATLAB environment, and in-house MATLAB functions. The continuous EEG data were re-referenced to the average of the left and right external mastoid signals to avoid biasing the data towards one hemisphere (Nunez and Srinivasan, 2006, Luck, 2014). The data was filtered using a digital zero-phase shift band-pass filter of 0.5-30Hz with a slope of 24 dB/octave. Then the continuous EEG data were epoched into 1-second segments (-200 to 800ms relative to stimulus onset), and the pre-stimulus interval (-200 to 0ms) was used as the baseline. We did not extend the epoch beyond 800ms, as previous studies have suggested the termination of LPP effects at 800ms (Schupp et al., 2000, Hu et al., 2014). The data were then baseline corrected by subtracting the average activity during the baseline period. Trials that had blinks in any part of the segment were excluded using a blink detection tool from ERPLab (<http://erpinfo.org/erplab>), in which vertical ocular artifacts exceeding a normalized cross-variance threshold of 0.7 were detected during the whole epoch (Lopez-Calderon and Luck, 2014, Luck, 2014). We rejected these trials because blinks might not only alter the sensory input of that trial, but also contaminate the EEG signals, especially the signals from the frontal channels. Epochs with saccadic eye movements were detected and discarded using a step-like artifact-detection function, in which horizontal ocular artifacts exceeding 70 μ V in amplitude were detected during the entire epoch with 200ms moving window and 50ms increment steps. This function is suitable to detect saccadic eye movements that typically consist of sudden, step-like changes in voltage (Lopez-Calderon and Luck, 2014). Remaining artifacts were further detected using a moving-window peak-to-peak artifact-detection method on specific midline electrodes. Epochs were excluded if the peak-to-peak voltage (the difference between the largest and smallest values) exceeded a threshold of 100 μ V. Bad channels were interpolated using the average voltage from their surrounding electrodes. Consequently, 24.0 \pm 13.8% (mean \pm SD) of trials was discarded from further analysis.

Importantly, after excluding trials due to artifacts, the average number of valid trials was similar at each morph level (one-way repeated-measure ANOVA, $F(6,132)=1.16$, $P=0.33$,

$\eta_p^2=0.05$). The number of trials from unambiguous happy face to unambiguous fearful face was 26.91 ± 5.85 (mean \pm SD), 27.08 ± 4.99 , 26.56 ± 4.67 , 25.95 ± 5.28 , 25.86 ± 5.01 , 25.65 ± 5.89 , and 26.26 ± 5.88 , respectively. For increasing ambiguity levels, the number of trials was 53.17 ± 11.14 , 52.74 ± 10.19 , and 78.39 ± 14.15 , respectively. Given that different numbers of morph levels were combined into ambiguity levels (thus different numbers of trials across the three ambiguity levels; see Fig. 1B), to control for any bias in trial number, we also repeated our analysis by randomly selecting an equal number of trials from each ambiguity level and found qualitatively the same LPP effects ($F(2,44)=10.9$, $P=1.46\times 10^{-4}$, $\eta_p^2=0.33$). Furthermore, we repeated our artifact rejection using independent component analysis (ICA) and we derived qualitatively the same results. Artifact rejection using ICA was employed in the speeded version of the task.

Because the LPP is a very slow potential and susceptible to artifacts from high-pass filtering (Tanner et al., 2015), we further confirmed our results using lower cutoffs (0.1Hz and 0.01Hz) of the high-pass filter and derived qualitatively the same results.

EEG: stimulus-locked event-related potential (ERP) analysis

Within each subject, mean waveform of each morph level was computed, time-locked to the onset of the stimulus. Single-subject mean waveforms were subsequently averaged to obtain group-level mean waveforms. Here, we measured the LPP (entire waveform) based on the time window of 400 to 700ms after stimulus onset at the parietal-central (Pz) electrode (Sabatinelli et al., 2007). Importantly, the scalp topography of the difference waveform between high ambiguity and unambiguous stimuli showed the most pronounced difference at Pz in this time window (Fig. 2A). To link the processing of ambiguous stimuli with later button response, we first compared the LPP from the same ambiguity level but with different RTs by splitting trials at each ambiguity level into long and short RT categories based on median splits. We then compared the LPP from different ambiguity levels but with similar RTs by selecting faster half trials from a more ambiguous group and slower half trials from a less ambiguous group. Group-level mean waveforms were calculated for each ambiguity-RT category.

EEG: time frequency analysis

To ensure that edge effects would not contaminate our windows of interest (from 200ms pre-stimulus to 800ms post-stimulus), we used a longer epoch window of -1000 to 2000 ms for frequency analysis. A Morlet wavelet transform (MWT) was performed, in which the cycle number linearly increased with frequency (Fuentemilla et al., 2006). A minimum of 1 cycle was used at the lowest frequency with a wavelet parameter of 0.65, to obtain better frequency resolution at higher frequencies (Delorme and Makeig, 2004). Within the epoch, 200 time points were generated. Fifty-nine linearly spaced frequencies were estimated from 1.0Hz to 30.0Hz for each trial. To eliminate the bias in the number of trials from different conditions, we first equalized the number of trials across conditions, and then used a common mean baseline spectrum (starting from -400 ms to -200 ms before stimulus onset) for all three ambiguity levels. This baseline period differed from that used for ERP analysis to avoid the edge effects. Then, the spectra were log-transformed (the unit of log-transformed spectrum is Decibel (dB)), and for each frequency, the corresponding average

baseline spectral power was subtracted, yielding the baseline-normalized event-related spectral perturbation (ERSP), an estimate of mean event-related changes in the power spectrum. Then ERSPs were averaged separately for each condition, and plotted at all frequencies, at time points from 200ms before stimulus onset to 800ms after stimulus onset. The mean activity was assessed between 100 and 300ms for theta (4-7Hz), and 400 to 700ms for delta (1-4Hz), alpha (8-12Hz) and beta (13-25Hz) frequency bands. We selected these frequency bands based on previous EEG studies about perceptual decisions, in which strong oscillatory activities have been observed (Sabatinelli et al., 2007, Fahrenfort et al., 2012, Cravo et al., 2013, Kelly and O'Connell, 2015).

EEG: source localization using Classical LORETA Analysis Recursively Applied (CLARA)

We estimated cortical sources for the LPP using Classical LORETA Analysis Recursively Applied (CLARA), a distributed source imaging method based on Low Resolution Electromagnetic Tomography (LORETA) (Pascual-Marqui et al., 1994). Analyses were conducted using the BESA 6.0 software package (BESA GmbH, Gräfelfing, Germany). Averaged ERP difference waveforms (unambiguous minus high ambiguity) from all channels were used to obtain the source model. The source location was estimated by the best correspondence between the recorded and estimated scalp distribution and subsequently transformed to a four-shell ellipsoidal head model. Our model used singular value decomposition (SVD) regularization with a cutoff of 0.005% and a default two-iteration scheme to perform the CLARA source imaging analysis. The locations and strengths of the regional sources were obtained for a series of 40ms time intervals within the time window of the LPP. Here, we selected four periods for analysis (280-320ms, 420-460ms, 560-600ms, and 660-700ms). We selected these four periods because they showed the largest variance of the LPP and they covered the entire LPP time window. The mean image in each period was computed and displayed. Source locations were finally transformed to the standard Talairach space.

EEG: source localization using dipole fitting

Besides the distributed source imaging method, we also applied a discrete source method to estimate the regional source of ERP components with a certain number of dipoles (Scherg, 1990). A current dipole is specified by its localization, orientation, and strength. Once the estimated dipoles are obtained, the corresponding model undergoes empirical evaluation of its ability to explain the recorded scalp topography by calculating the residual variance (RV) of the signal, i.e., the percentage of variance in scalp topography that cannot be explained by the fitted dipoles.

To estimate the sources of the average LPP difference (unambiguous minus high ambiguity), a principal component analysis (PCA) was employed first to estimate the minimal number of dipoles. In our data, four dipoles could explain more than 97.3% variance during the time interval of 400 to 700ms after stimulus onset, and we thus used five dipoles (4 fixed dipoles and 1 free dipole). The four fixed dipoles were obtained from the CLARA estimation (around the anterior cingulate cortex, posterior cingulate cortex, insula, and paracentral lobule), and they were also informed by previous neuroimaging reports and meta-analysis (Huettel et al., 2006, Krain et al., 2006). The dipole configurations were accepted when the

five-dipole model resulted in <10% RV (for the time interval of 400 to 700ms after stimulus onset). Finally, the source location of each dipole was transformed to the standard Talairach space.

Functional magnetic resonance imaging (fMRI): imaging acquisition

MRI scanning was conducted at the South China Normal University on a 3-Tesla Tim Trio Magnetic Resonance Imaging scanner (Siemens, Germany) using a standard 12-channel head-coil system. Whole-brain data were acquired with echo planar T2*-weighted imaging (EPI), sensitive to blood-oxygen-level dependent (BOLD) signal contrast (31 oblique axial slices, 3 mm-thicknesses; TR = 2000ms; TE = 30ms; flip angle = 90°; FOV = 224mm; voxel size: 3 × 3 × 3mm). T1 weighted structural images were acquired at a resolution of 1 × 1 × 1mm.

fMRI: imaging analysis

Neuroimaging data were preprocessed and analyzed using SPM8 (www.fil.ion.ucl.ac.uk/spm/). The first 4 volumes were discarded to allow the MR signal to reach steady-state equilibrium. EPI images were sinc interpolated in time to correct for slice-timing differences and realigned to the first scan by rigid-body transformations to correct for head movements. Utilizing linear and nonlinear transformations, and smoothing with a Gaussian kernel of full-width-half maximum 6 mm, EPI and structural images were coregistered to the T1 MNI 152 template (Montreal Neurological Institute, International Consortium for Brain Mapping). Global changes were removed by high-pass temporal filtering with a cutoff of 128s to remove low-frequency drifts in signal.

We used an event-related design. In the general linear model (GLM) design matrix, for every subject we estimated a GLM with autoregressive order 1 [AR(1)] and the following regressors (R): R1 at face presentation; R2 at face presentation modulated by fear levels: 100%, 70%, 60%, 50%, 40%, 30%, 0%; R3 at face presentation modulated by ambiguity levels: unambiguous, 30%/70% morph (intermediate ambiguity), 40%-60% morph (high ambiguity); and R4 at fixation presentation. Because both the reaction time (RT) and ambiguity levels were correlated with confidence, we also repeated the analysis by adding the z-normalized RT (for each subject) as one additional modulator and orthogonalized it to earlier modulators using the default SPM orthogonalization function. We derived similar results when adding RT as a modulator.

For all GLM analyses, six head-motion regressors based on the SPM's realignment estimation routine were added to the model (aligned to the first slice of each scan). Multiple linear regressions were then run to generate parameter estimates for each regressor for every voxel. The contrast (difference in beta values) images of the first-level analysis were entered into one-sample t-tests for the second-level group analysis conducted with a random-effects statistical model (Penny and Holmes, 2004). Activations were reported if they survived $P < 0.001$ uncorrected, cluster size $k > 10$. For amygdala, we restricted our analysis to an anatomically defined region obtained from the WFU PickAtlas (<http://fmri.wfubmc.edu/software/PickAtlas>). Activations were reported if they survived $P < 0.05$ FWE after small volume correction.

Results

Behavioral results

In the main experiment with fear-happy morphed faces, we asked subjects to judge emotional faces as fearful or happy (Fig. 1A). Faces were either unambiguously happy, unambiguously fearful, or graded ambiguous morphs between the two emotions (Fig. 1B). Since emotion ambiguity was distributed symmetrically between the two emotions, we grouped the seven emotion levels into three ambiguity levels (Fig. 1B): unambiguous, intermediate (30%/70% morph), and high (40%-60% morph). In later control experiments with independent subjects (see below), we used an analogous protocol, but instead of fear-happy morphed faces we used anger-disgust morphed faces and cat-dog morphed animals (Fig. 1B).

For each subject, we quantified behavior as the proportion of trials identified as fearful as a function of morph level (Fig. 1C). We found a monotonically increasing relationship between the likelihood of identifying a face as fearful and the fearfulness in the morphed face for all subject groups (Fig. 1C). Three subject groups (behavioral, EEG, and fMRI) from the main experiment with fear-happy morphed faces had similar psychometric curves (point-by-point comparison using one-way ANOVA, corrected for false discovery rate (FDR) for $q < 0.05$ (Benjamini and Hochberg, 1995); all $P_s > 0.05$). We further quantified each psychometric curve using an emotion judgment index (EJI): the morph levels (in units of % fearful) at which subjects were equally likely to judge a face as fearful or happy. Again, we found no significant difference between subject groups (one-way ANOVA: $F(2,64) = 0.008$, $P = 0.99$, $\eta_p^2 = 0.03$), showing that all subject groups made similar emotion judgments. A logistic mixed model further confirmed our results and revealed a bias towards fearful judgments for ambiguous faces (Supplementary Results).

We acquired confidence ratings from behavioral subjects after they reported a face as fearful or happy. Subjects reported significantly higher levels of confidence for unambiguous faces compared to ambiguous faces (Supplementary Fig. 1A1, A2; see Supplementary Results for statistical details). In addition to the explicit confidence ratings, the RT (relative to stimulus onset) for the fear/happy decision can be considered as an implicit measure of confidence because it showed a similar pattern as the explicit ratings (Supplementary Fig. 1A3, A4). RT was faster for unambiguous faces compared to ambiguous faces for all three subject groups (Fig. 1D, E for all subjects and Supplementary Fig. 1A–C for each subject group). Note that the behavioral patterns of all three subject groups were comparable, although EEG and fMRI subjects did not provide confidence ratings. Taken together, both explicit confidence ratings and implicit confidence measures by RT demonstrated a systematic relationship with perceptual ambiguity: the more ambiguous, the lower the confidence and the longer time it took to process the ambiguous information.

A late positive potential (LPP) is associated with ambiguity processing

What are the neural substrates underlying ambiguity processing? We next conducted an EEG study using the same task and stimuli with 23 healthy subjects. Previous findings argue that a late positive potential (LPP) originating from the parietal-central (Pz) electrode is involved

in affective valence (pleasant, unpleasant, and neutral) and/or arousal processing (see Introduction). Our own data similarly showed a strong late positivity to unambiguous faces with strong emotions (Fig. 2A). Moreover, we found that this LPP component showed a parametric relationship with the degree of ambiguity shown in the stimuli, suggesting that LPP amplitude can index the level of perceptual ambiguity (Fig. 2B–E). Given the spatial and temporal results shown in Fig. 2, we focused on the electrode Pz during the time interval of 400 to 700ms after stimulus onset, consistent with prior literature on the LPP (Pastor et al., 2008, Leite et al., 2012).

As expected, a clear LPP component was observed for all 7 morph levels (Fig. 2B) and the mean LPP amplitude varied systematically as a function of morph levels (Fig. 2C; see figure legend for statistical details). Notably, the LPP appeared insensitive to the type of emotion shown (i.e., the unambiguous fearful face had a similar LPP as the unambiguous happy face), but instead varied systematically as a function of emotion ambiguity. We next grouped all trials into three ambiguity levels and found that the LPP could differentiate ambiguity in faces as early as 470ms, with unambiguous faces showing the strongest positivity (Fig. 2D). Post-hoc t-tests on the mean LPP amplitude (Fig. 2E) revealed a significant difference between unambiguity and intermediate ambiguity (paired two-tailed t-test, $t(22)=3.17$, $P=0.004$, Cohen's $d=0.68$), and a marginal difference between intermediate and high ambiguity ($t(22)=1.73$, $P=0.098$, $d=0.37$).

In addition to ERP, time-frequency analysis also revealed neural oscillations in the delta frequency band that parametrically encoded levels of ambiguity (Fig. 2F–H; Supplementary Results).

It is worth noting that in order to better dissociate perception and decision, our subjects were only allowed to respond after the offset of the stimulus. However, we observed qualitatively the same results when using a fully speeded version of the task (Supplementary Fig. 2C–E).

Taken together, we show that the LPP plays a crucial role in processing perceptual ambiguity.

The LPP is associated with judgment decisions rather than stimulus representations

We have shown that the LPP is associated with ambiguity processing, but it remains unclear what processing stage this might correspond to. Is it associated with perceptual representation of the stimulus or with making judgments about the stimulus in our task? To answer this question, we next analyzed the LPP in relation to the time taken to make decisions (RT), broken down for ambiguity levels. If the LPP represents stimulus perception, it should vary with ambiguity levels in the stimulus regardless of RT. On the other hand, if it encodes decisions, it should vary with RT regardless of stimulus ambiguity.

Both RT (Fig. 1D, E) and the LPP (Fig. 2C, E) varied systematically as a function of ambiguity, indicating that the LPP might be associated with emotion judgment decisions. Indeed, when we partitioned each subject's LPPs into four equal portions according to RT quartiles (shortest vs. short vs. long vs. longest RT), we found a significantly greater LPP amplitude for shorter RT (Fig. 3A), suggesting that the LPP was strongly associated with

behavioral response. We also found that the LPP increased amplitude in steps with decreasing RT quartiles (Fig. 3A; paired t-test between adjacent conditions).

To dissociate the LPP's role in encoding stimulus and decisions, we first separated LPPs at each ambiguity level into two groups according to RT (sorted by the median RT): a long RT group vs. a short RT group, so that we could examine different RTs with the same level of ambiguity. ERPs with a shorter RT had a greater LPP at each ambiguity level (Fig. 3B, C), suggesting that keeping the stimulus constant, significantly greater LPPs were indeed associated with significantly faster decisions.

We next held RT constant but examined the LPP under different levels of ambiguity. We selected trials from different ambiguity levels so that they had similar RTs (e.g., a longer RT group in the unambiguous condition vs. a shorter RT group in the intermediate ambiguity condition, and a longer RT group in the intermediate ambiguity condition vs. a shorter RT group in the high ambiguity condition). We found remarkably similar LPPs given similar RTs (Fig. 3D, E). Therefore, keeping the RT constant, similar LPPs were associated with similar RTs regardless of ambiguity levels in stimulus.

Together, our data suggest that the LPP encodes decisions under ambiguity rather than stimulus representation.

Single-trial analysis and linear mixed models reveal a trial-by-trial coupling between the LPP and RT

To directly capture the trial-by-trial variation in the LPP and RT, we also conducted a single-trial analysis, which revealed a trial-by-trial coupling between the LPP and RT (Supplementary Fig. 3; Supplementary Results). In addition, we constructed a linear mixed model (LMM) to analyze the relationship between RT (excluding RTs < 1100ms; log-transformed) and single-trial LPP amplitude (mean LPP in the time interval 400 to 700ms after stimulus onset) among all subjects. First, we used RT as the fixed effect and by-subject random intercept as well as by-subject random slopes as random effects. Statistical significance of the model was computed by likelihood ratio tests of the full model with the fixed effect of RT against a null model without the fixed effect of RT. We found that in the full model RT could predict LPP amplitude with a significant regression coefficient (slope; $\beta = -1.06$, $P < 0.001$) and intercept ($\beta = 10.87$, $P < 0.001$), and the full model with the fixed effect of RT significantly outperformed the null model ($\chi^2(6) = 11.34$, $P < 0.001$), suggesting that the variance of LPP amplitude could be well explained by the variance of RT. Second, we built another model with LPP amplitude as the fixed effect, but still with by-subject random intercept as well as by-subject random slopes as random effects. We found that the LPP amplitude could also predict RT with a significant regression coefficient ($\beta = -0.005$, $P < 0.001$) and intercept ($\beta = 5.83$, $P < 0.001$), and the full model with the fixed effect of LPP amplitude significantly outperformed the null model ($\chi^2(6) = 11.05$, $P < 0.001$), suggesting that the variance of RT could also be explained by the variance of LPP amplitude.

Together, the strong coupling between the LPP and response latency supports that the LPP encodes behavioral decisions.

A mediation model formally captures the relationship between the LPP and RT

The above results suggest that the effect of stimulus ambiguity on RT is mediated by the LPP. To directly test whether the single-trial relationship between stimulus ambiguity and RT was formally mediated by the LPP, we next constructed a three-variable path model (MacKinnon et al., 2006) with stimulus ambiguity as the predictor, RT as the outcome, and the LPP amplitude (mean LPP in the time interval 400 to 700ms after stimulus onset) as the mediator variable (Fig. 3F). We used the data from the fully speeded version of the task (Supplementary Fig. 2C–E) because it had a tighter relationship between the LPP and RT. In this model, stimulus ambiguity was a reliable predictor of the LPP amplitude ($a=-1.18$, $P<0.001$) and the mediation effect of the LPP amplitude on RT was also significant ($b=-5.56$, $P<0.001$), showing that the LPP could mediate the decision process (mediation effect ($c-c'$) = 6.68 ± 1.12 (mean \pm SEM), 95% CI = [4.67 9.07]; Sobel test with 5000 bootstraps: $Z=6.01$, $P<0.001$; $P_m = 10.75\%$). Qualitatively the same results were derived using Z-scored RT and log-transformed RT.

Control experiments confirm the specificity of the LPP for only decisions under ambiguity

To experimentally test the mediation effect of the LPP on decision in the above mediation model, we next used two control experiments with 15 healthy subjects to reveal a direct relationship between the LPP and behavioral response to ambiguity. We hypothesized that if the LPP is specifically associated with the decisions under ambiguity, it or its effect on ambiguity will disappear when no decisions are made or when decisions are not under ambiguity. We still focused on the electrode Pz in the same time interval (400 to 700ms after stimulus onset) as all previous analyses.

In the first control experiment (Control Experiment 1), subjects passively viewed the faces without making any decisions about facial emotions. Indeed, we found a strongly reduced LPP (Fig. 4A) and no difference in the LPP interval for ambiguity levels using the mean amplitude (Fig. 4A).

In the second control experiment (Control Experiment 2), subjects judged whether the stimulus was a human face or an animal (see Materials and Methods). Although both the face and animal stimuli were ambiguous (ambiguity between anger/disgust for the face, and ambiguity between cat/dog for the animal; Fig. 1B), decisions/judgments about such stimuli in this control experiment were unrelated to the dimensions on which the stimuli were ambiguous, instead requiring a classification that could be made equally easily for all exemplars in that category. Again, for both types of stimuli, we found a strongly reduced LPP (Fig. 4B, C) and no difference in the LPP interval for ambiguity levels using the mean amplitude (Fig. 4B, C). Therefore, our results here once again showed that the LPP did not represent stimulus ambiguity because our stimuli were indeed ambiguous. To further examine the relationship between the LPP and RT, we repeated the above single-trial analysis: we found that when RT was similar across stimulus ambiguity levels (face: $F(2,28)=0.35$, $P=0.71$, $\eta_p^2=0.025$; animal: $F(2,28)=2.34$, $P=0.12$, $\eta_p^2=0.14$), the correlation between the LPP and RT was not biased towards negative as in the main task (one-tailed t-test of correlation coefficient r against 0: face: $t(14)=1.02$, $P=0.33$, $d=0.27$; animal:

$t(14)=1.56$, $P=0.14$, $d=0.42$), suggesting that the LPP was not systematically associated with RT anymore.

It is worth noting that using the same stimuli, when decisions were related to the ambiguous aspect of the stimuli, we did observe a robust LPP that could differentiate levels of ambiguity (Supplementary Results). This result not only supported the finding from the main experiment, but also suggested that the LPP encoded perceptual ambiguity in a domain-general fashion (i.e., both in the case of emotion ambiguity for the face stimuli, as well as in the case of animal ambiguity for the cat/dog stimuli).

Taken together, we have shown that when no decisions are made about ambiguity, the LPP is strongly reduced, even when the stimuli are still ambiguous. Our results show a direct evidence that the LPP is specifically involved in decisions under ambiguity.

Context of ambiguous stimuli modulates the LPP

We next explored how the LPP emerged and developed and whether the LPP was influenced by context, which could be considered as a moderator of the statistical mediation model (Fig. 3F). To answer these questions, we designed a 3-block experiment (Control Experiment 3): in the first block, subjects only judged unambiguous faces; in the second block, subjects judged both unambiguous and morphed faces; and in the third block, subjects again only judged unambiguous faces. With this design, we could examine how ambiguous morphed faces influence the LPP associated with the unambiguous faces. Thirty-two healthy subjects participated in this study. In 16 subjects, there were no breaks between blocks, and in 16 subjects, there were 2-minute breaks between blocks.

Behaviorally, we found no difference in discrimination accuracy for each block (Fig. 5A). In the second block, we replicated our previous finding that higher ambiguity led to slower judgments (Fig. 5C). However, we found no difference in RT for the same unambiguous faces across three blocks (Fig. 5B), indicating that face judgment behavior was not influenced by the context of stimuli.

Neuronally, we still observed an LPP that differentiated levels of ambiguity in the second block (Fig. 5D). Notably, the LPP was still present for unambiguous faces alone in the first and third block (Fig. 5D). However, the LPP of unambiguous trials was much weaker when there were no ambiguous trials, suggesting that the LPP was modulated by the context of ambiguous stimuli. Post-hoc t-test on the mean LPP amplitude (Fig. 5E, F) revealed a significant difference of unambiguous faces between the first and second block (paired two-tailed t-test, $t(31)=3.01$, $P=0.0052$, $d=0.55$), as well as between the second and third block ($t(31)=3.05$, $P=0.0046$, $d=0.55$). However, there was no significant difference of unambiguous faces between the first and third block ($t(31)=0.39$, $P=0.70$, $d=0.07$), suggesting that the influence of the ambiguous stimuli in the second block was transient and did not carry over into the third block.

In the above results, we collapsed the conditions with and without breaks. However, we observed qualitatively the same results when we analyzed each condition separately (Supplementary Fig. 4), showing that subjects could adapt rapidly to the presence and

absence of the ambiguous stimuli, even if there were no breaks for subjects to adjust between blocks. This also supported that the influence of the ambiguous stimuli was transient in the second block.

Source localization of the LPP components

We have characterized the nature of the LPP in the above sections. But where does this signal originate? We next conducted a source localization of the LPP in four 40ms time windows using a distributed model (Fig. 6A). The mean LPP difference waveforms (unambiguous minus high ambiguity) were localized to four main regional sources—the vACC (peak: Montreal Neurological Institute (MNI) coordinate: $x=-10$, $y=51$, $z=10$), PCC ($x=10$, $y=-42$, $z=26$), paracentral lobule ($x=10$, $y=-36$, $z=50$), and insula ($x=40$, $y=-6$, $z=-4$). These localized sources are consistent with previous studies showing that the vACC encodes confidence in the judgment (i.e., the less ambiguous the stimulus, the more confident the judgment and thus the higher vACC activity) (De Martino et al., 2013, Lebreton et al., 2015) (see Discussion for more details), the PCC is implicated in focused attention (Garrison et al., 2013), while the paracentral lobule is associated with sensorimotor functions (Wiemer and Pauli, 2016).

We further confirmed our results using a discrete model, in which one free dipole and four fixed dipoles (the vACC, PCC, insula, and paracentral lobule indicated from the distributed model) were used (Fig. 6B). Our model could explain 90.86% of the variance of the scalp voltage in the interval of 400 to 700ms after stimulus onset (residual variance (RV)=9.14%). The free dipole was localized to the striatum (putamen) ($x=20$, $y=12$, $z=-10$), which has been reported in decision making under risk and ambiguity (Hsu et al., 2005, Yoshida and Ishii, 2006).

Functional neuroimaging

To further validate the source localizations, we conducted an fMRI study with 19 healthy subjects using the same stimuli and task. On the one hand, we found a significant increase of BOLD signal in the bilateral inferior frontal gyrus (IFG)/anterior insula and dorsal medial prefrontal cortex (dmPFC)/dACC with increasing level of ambiguity regardless of emotion intensity (Fig. 6C, E and Supplementary Table 1); on the other hand, we found a significant increase of BOLD signal in the left vACC, PCC, dorsolateral prefrontal cortex (dlPFC), inferior parietal lobule (IPL), and right postcentral gyrus with decreasing level of ambiguity (Fig. 6D, F and see Supplementary Table 1 for all areas). Notably, the vACC, PCC and insula were very consistent with the regional sources of the LPP (Fig. 6A), providing further evidence that the LPP was generated from these areas.

Source waveforms from the vACC and IFG encode ambiguity levels

To further confirm that the regions identified by fMRI (Fig. 6C, D and Supplementary Table 1) generated ERPs that encoded ambiguity, we next predicted source waveforms from ROIs identified by fMRI (Fig. 6G; left dmPFC, left IFG/insula, right IFG/insula, left vACC, left PCC, right postcentral gyrus, and a free dipole) using the discrete model. Mean source amplitude in the LPP interval (400-700ms after face onset) indeed varied significantly as a function of ambiguity, with the left vACC showing the most positive potential for

unambiguous faces, whereas the left IFG/insula and the right IFG/insula showing the most negative potential for unambiguous faces (Fig. 6H), consistent with both the LPP and fMRI findings. Mean source amplitude in the other ROIs identified by fMRI also showed a trend consistent with the LPP and fMRI results, although they did not reach a statistical significance. Pooled signals from all ROIs predicted waveforms consistent with the LPP (Fig. 6I, J; $F(2,44)=9.81$, $P=3.0\times 10^{-4}$, $\eta_p^2=0.98$). In conclusion, we confirmed that the regions identified by the fMRI could generate ERPs that encode ambiguity.

Discussion

We used three types of ambiguous stimuli (fear-happy morphed faces, anger-disgust morphed faces, and cat-dog morphed animals) to examine the neural representation of perceptual ambiguity. Behaviorally, higher ambiguity led to slower judgments and lower confidence. Neuronally, a late positive potential, the LPP, differentiated levels of ambiguity and showed the highest amplitude for the least ambiguous stimuli. When controlling for levels of ambiguity and levels of RT, we found that the LPP was associated with behavioral judgment about ambiguity rather than perceptual representations of the ambiguous stimuli. This finding was further corroborated by single-trial correlation between the LPP amplitude and RT and a linear mixed model, and formally captured by a statistical mediation model. Two control experiments directly testing the mediation model showed that the LPP was abolished if no response was made or if the judgment was not about ambiguity. Furthermore, another control experiment showed that a stronger LPP arose in the context of ambiguous stimuli, revealing a moderator of the mediation model. Lastly, through source modeling, we revealed that the LPP component encoding ambiguity originated from the cingulate cortices and insula, and we further confirmed the results using fMRI and fMRI-guided ERP source prediction. Taken together, our findings suggest a context-dependent role for the LPP in linking perceptual ambiguity to behavioral choice, which may in turn reflect decision conflicts and mental effort to resolve such conflicts.

Possible caveats

Comparing between the tasks with and without decisions using the identical stimuli (Control Experiment 1; Fig. 4A), the abolished LPP in the passive viewing could be due to reduced attention. However, also using the identical stimuli but with different decision questions (Control Experiment 2; Fig. 4B, C; Supplementary Results), and importantly with all tasks having judgment responses, the LPP did not emerge with decisions about unambiguous choices, arguing against a simple role of attention (the stimulus should be equally attended when asking for a judgment of it). Nonetheless, we acknowledge that task difficulty, attention, and RT are of course all intercorrelated to some extent, and future studies will be needed to further distinguish attentional effects. Similarly, examining unease/anxiety caused by ambiguity in decisions will be a clear future direction.

Furthermore, we found that the context of ambiguous stimuli did not modulate reaction times in judging unambiguous faces (Fig. 5B) but the amplitude of the LPP (Fig. 5E), indicating that the association between the LPP and decisions was also dependent on the context. A stronger LPP only emerged when subjects found that ambiguous stimuli were

present, but the LPP quickly diminished when subjects found that only unambiguous stimuli were present (Control Experiment 3; Fig. 5D). Such transient enhancement of the LPP might result from enhanced attention, consistent with the LPP's sensitivity to voluntary control and attentional modulation (Ferrari et al., 2008, Hajcak et al., 2009). This also demonstrates a functional role of the LPP that monitors ambiguity in the context.

It is worth noting that our present data have shown evidence for both a mediation by the LPP, and the mediation weights were further moderated by context (the presence of ambiguous stimuli). Although in our model the LPP was regarded as the mediator for RT (Fig. 3F), it is also likely that RT mediates the effect of stimulus ambiguity on the LPP. A model with RT as the mediator revealed a similar effect.

The LPP and its sources

It is worth noting that different terms have been used to describe the LPP and responses close in time, including P300, P3, centro-parietal positive potential (CPP), late positive deflection (LPD), and late positive component (LPC). Furthermore, the P300 has two subcomponents: P3a and P3b (see (Polich, 2007) for a detailed review). The P3a is a more frontally distributed, earlier component elicited by salient oddball stimuli that are not necessarily task-relevant but are novel (e.g., an infrequent distinct tone presented in a series of frequent tones without a task can produce the P3a), whereas the P3b originates from temporal-parietal activity associated with attention and is elicited by task-relevant stimuli during target stimulus processing. Given that the LPP is specifically associated with task-relevant stimuli (it was abolished in Control Experiment 1), consistent with its absence for irrelevant stimuli shown in (O'Connell et al., 2012), we argue that the LPP is more equivalent to the P3b subcomponent.

Consistent with our source localization results, prior studies have suggested that the LPP arises from a distributed brain network, including the ACC, PCC, and insula (Liu et al., 2012, Peng et al., 2012, Yoder and Decety, 2014) (also see (Weinberg et al., 2013)). Direct electrocortical stimulation of the prefrontal cortex during emotional picture presentation disrupts arousal modulation of the LPP over posterior electrode sites (Hajcak et al., 2010). Using a simultaneous EEG and fMRI, the LPP amplitude is significantly correlated with BOLD activity in visual cortices, temporal cortices, amygdala, orbitofrontal cortex, and insula (although there are category-specific differences in such coupling) (Liu et al., 2012). Moreover, an MEG homolog of the LPP is localized within bilateral occipitoparietal and right prefrontal cortex (Moratti et al., 2011). Although it is arguable that scalp EEG can be source localized to the striatum (Cohen et al., 2011), a study using simultaneous EEG and fMRI revealed that a larger LPP amplitude is correlated with a higher ventral striatum response, suggesting the striatum as one of the sources for the LPP (Pfabigan et al., 2014).

The LPP and perceptual decisions

Simple perceptual decisions can generally be broken down into three main processing stages: sensory encoding, decision formation and motor execution (Sternberg, 1969). Consistent with the present study, the LPP is specifically linked with making decisions (see (Kelly and O'Connell, 2015) for a review): it is evoked exclusively by task-relevant events

requiring decisions (Sutton et al., 1965b, Hillyard et al., 1971) and its timing varies closely with RT (Ritter et al., 1972, Kutas et al., 1977). RT reflects conflicts in judgment and is inversely correlated with decision certainty (Kiani et al., 2014), and the LPP may thus index judgment difficulty and reflect mental effort to resolve such conflicts. In contrast to (O'Connell et al., 2012), which shows that (1) the peak latency of the LPP is inversely proportional to RT, (2) the peak LPP amplitude is constant, and (3) action execution is determined by LPP amplitude reaching a threshold or criterion level, we found in the present study that levels of ambiguity were encoded by LPP amplitude but not latency, and the LPP amplitude was inversely correlated with RT (i.e., the greater the LPP, the faster the RT, regardless of stimulus). Our results thus argue against a simple accumulation-to-bound model.

Notably, in order to better dissociate perception and decision, our subjects were only allowed to respond after the offset of the stimulus (the task was not fully speeded), therefore, they might make their decisions well before executing the button press. However, a fully speeded version of the task still replicated the results. On the other hand, different neural substrates may collectively produce the LPP during this process, and different brain areas may have different latencies and weights across time (Fig. 6A). However, given our task protocol, our data can rule out the possibility that responses could truncate the LPP process, a confound that, if it were present, would also predict that short RTs are associated with weaker LPPs, while we found exactly the opposite.

It has been suggested that the LPP is a product of both an automatic facilitation of perceptual activity and post-perceptual processing under cognitive control (Moratti et al., 2011). However, our results argued that the LPP was predominantly involved in post-perceptual decisions rather than perceptual representation of stimuli. Consistent with the present result, in an instrumental learning task, a similar parietal ERP component as the LPP encodes the certainty of the impending response and is predictive for the decision on the next trial (Fischer and Ullsperger, 2013).

The LPP and ambiguity

In this study, we showed that the LPP differentiated levels of ambiguity. This is consistent with several studies showing that the LPP can differentiate racially ambiguous faces (Willadsen-Jensen and Ito, 2006), ambiguous smiles (Calvo et al., 2013), and inconsistency of traits (Cacioppo et al., 1994). Many studies have also shown that the LPP is modulated by emotional intensity and arousal and thus reflects an enhanced perception of emotional stimuli (Cuthbert et al., 2000, Schupp et al., 2000, Sabatinelli et al., 2007, Leite et al., 2012), although our results showed that the LPP varied as a function of emotion ambiguity, instead of emotion intensity or arousal (Wang et al., 2017), and as a function of stimuli even without any emotional content (cat-dog morphs). This is likely because different processes can generate a similar LPP, or the affective stimuli used in previous studies also require different levels of mental efforts for judgments (i.e., emotion intensity/arousal co-vary with mental efforts).

In a prior study, we used the same task and found that single neurons and BOLD-fMRI in the amygdala encode levels of perceptual ambiguity (Wang et al., 2017). However, patients

with focal amygdala lesions do not demonstrate any impairment in judging ambiguity and confidence. Given the ambiguity signal encoded in the cingulate cortex shown in the present study, we hypothesize that the cingulate cortex provides input to the amygdala for ambiguity judgment. Indeed, a preliminary DCM analysis has confirmed this hypothesis.

Functional neuroimaging reveals a distributed neural network encoding ambiguity and confidence

In this study, our fMRI data revealed a significant increase of BOLD signal with increasing emotion ambiguity in the bilateral IFG, dmPFC, and dACC, which is very consistent with a previous study showing that the imaging contrast between ambiguous and clear facial expressions induces activation in the dACC, dmPFC and IFG (Nomura et al., 2003). Furthermore, ambiguous emotional faces relative to unambiguous emotional faces activate regions implicated in conflict monitoring and cognitive control, including the dACC, dlPFC, and IPL (Simmons et al., 2006), and intolerance of emotion ambiguity correlates with insula activation (Simmons et al., 2008). More generally, inferring perceptual ambiguity activate bilateral IFG (Sterzer and Kleinschmidt, 2007), and ambiguous decision making is associated with activity in the dACC, vACC, dlPFC, and parietal cortex (Krain et al., 2006). Together, the neural network encoding perceptual ambiguity identified in our study has been supported by others.

Ambiguity can induce anxiety and relate to response conflict and mental efforts to resolve such conflict, and in particular ACC activation by ambiguity corroborates this idea. Notably, encoding of affect, pain and cognitive control converges on the dACC and all these three domains are similarly affected by manipulations of ambiguity (Shackman et al., 2011). It has been shown that unpredictable aversive events such as threat can activate both the dACC and vACC (Alvarez et al., 2011), whereas perceived controllability of pain attenuates pain-evoked dACC activity (Salomons et al., 2004).

Recent fMRI studies have shown an involvement of the vACC in integration of confidence (De Martino et al., 2013, Lebreton et al., 2015), consistent with our findings that vACC activity was positively correlated with decreasing level of ambiguity. The vACC encodes confidence even when no confidence judgment is required of the participants, suggesting that the integration of confidence is automatic in the vACC (Lebreton et al., 2015). Although our study did not distinguish between confidence and ambiguity (see (Pouget et al., 2016) for a recent review), our results further highlight the key role of the dACC in encoding low confidence/high ambiguity and the vACC in registering high confidence/low ambiguity distinctively, which may reflect functional segregations within the ACC (e.g., emotion appraisal in the dACC vs. regulation in the vACC) (Etkin et al., 2011). Lastly, the greater vACC activation for unambiguous stimuli may be associated with greater subjective values for unambiguous stimuli during decision making (Rushworth and Behrens, 2008, Bartra et al., 2013).

Multimodal methods

EEG and fMRI have complementary advantages with regard to their spatial and temporal resolution. On the one hand, fMRI-informed ERP-source modeling can constrain the

possible source locations of ERPs, thus providing superior spatial resolution compared with EEG; on the other hand, compared with the regional BOLD response, the resulting ERP-source waveforms produce more accurate information about the temporal evolution of activity in a network of cortical areas. This approach has a relatively long tradition (Heinze et al., 1994) and has been widely used in studying vision, emotion, and cognition (Debener et al., 2006). In particular, it has been shown that in viewing of emotional pictures, the amplitude of the LPP correlates significantly with BOLD intensity in lateral occipital, inferotemporal, and parietal visual areas across picture contents (Sabatinelli et al., 2007). It is worth noting that the above-mentioned studies, including ours, had EEG and fMRI conducted in separate sessions. Translating our task into simultaneous EEG-fMRI (Nguyen and Cunnington, 2014) will be an informative future direction.

Conclusions

Previous studies have shown that the LPP encodes decisions by integrating sensory evidence and determining actions through a boundary-crossing criterion, similarly across multiple different tasks (O'Connell et al., 2012, Kelly and O'Connell, 2013, Murphy et al., 2015). Our findings provide further specificity to this prior work: within each experiment, we dissociated levels of ambiguity in stimulus and levels of RT and showed that the LPP was associated with decisions under ambiguity rather than stimulus representation; across experiments, we also showed that similar LPPs were associated with similar RTs. Additional experiments directly tested the predictions from this result by experimentally manipulating whether or not decisions were made, and whether or not those decisions were about ambiguity. Taken together, we have shown compelling evidence that the LPP specifically encodes decisions about stimuli when the choice options classifying those stimuli are ambiguous. These results were formally captured by a statistical mediation model and we further revealed a moderator (presence of ambiguous stimuli) of this model.

Assessing decision ambiguity (internal) independent from perceptual ambiguity (external) is critical for decision making. Underestimating decision ambiguity may lead to overconfidence or impulsive choices, whereas overestimating decision ambiguity may make decision makers being indecisive. Our study identified a neural signature of perceptual decisions under ambiguity and may provide novel insights into many distortions of judgment, such as indecisiveness and impulsivity.

Supplementary Material

Refer to Web version on PubMed Central for supplementary material.

Acknowledgements

We thank Xiaojing Wu and Min Pu for collecting some of the data. This research was supported by the Autism Science Foundation to S.W., the National Natural Science Foundation of China (No. 31371128) and MOE Tier 1 (R-581-000-191-112) to R.Y., the Scientific Research Foundation of Graduate School of South China Normal University (2015wkxm02) and China Scholarship Council to S.Sun, and an NIMH Conte Center to R.A.. The funders had no role in study design, data collection and analysis, decision to publish, or preparation of the manuscript.

References

- Alexander WH, Brown JW (2010) Computational Models of Performance Monitoring and Cognitive Control. *Topics in Cognitive Science* 2:658–677. [PubMed: 21359126]
- Alvarez RP, Chen G, Bodurka J, Kaplan R, Grillon C (2011) Phasic and sustained fear in humans elicits distinct patterns of brain activity. *NeuroImage* 55:389–400. [PubMed: 2111828]
- Bach DR, Seymour B, Dolan RJ (2009) Neural activity associated with the passive prediction of ambiguity and risk for aversive events. *The Journal of Neuroscience* 29:1648–1656. [PubMed: 19211872]
- Bartra O, McGuire JT, Kable JW (2013) The valuation system: A coordinate-based meta-analysis of BOLD fMRI experiments examining neural correlates of subjective value. *NeuroImage* 76:412–427. [PubMed: 23507394]
- Benjamini Y, Hochberg Y (1995) Controlling the False Discovery Rate: A Practical and Powerful Approach to Multiple Testing. *Journal of the Royal Statistical Society Series B (Methodological)* 57:289–300.
- Cacioppo JT, Crites SL, Gardner WL, Berntson GG (1994) Bioelectrical echoes from evaluative categorizations: I. A late positive brain potential that varies as a function of trait negativity and extremity. *Journal of Personality and Social Psychology* 67:115–125. [PubMed: 8046583]
- Calvo MG, Marrero H, Beltrán D (2013) When does the brain distinguish between genuine and ambiguous smiles? An ERP study. *Brain and cognition* 81:237–246. [PubMed: 23262178]
- Cohen MX, Cavanagh JF, Slagter HA (2011) Event-related potential activity in the basal ganglia differentiates rewards from nonrewards: Temporospatial principal components analysis and source localization of the feedback negativity: Commentary. *Human Brain Mapping* 32:2270–2271. [PubMed: 21826758]
- Cole MW, Yeung N, Freiwald WA, Botvinick M (2009) Cingulate cortex: Diverging data from humans and monkeys. *Trends in Neurosciences* 32:566–574. [PubMed: 19781794]
- Cravo AM, Rohenkohl G, Wyart V, Nobre AC (2013) Temporal Expectation Enhances Contrast Sensitivity by Phase Entrainment of Low-Frequency Oscillations in Visual Cortex. *The Journal of Neuroscience* 33:4002. [PubMed: 23447609]
- Cunningham WA, Espinet SD, DeYoung CG, Zelazo PD (2005) Attitudes to the right-and left: frontal ERP asymmetries associated with stimulus valence and processing goals. *NeuroImage* 28:827–834. [PubMed: 16039143]
- Cuthbert BN, Schupp HT, Bradley MM, Birbaumer N, Lang PJ (2000) Brain potentials in affective picture processing: covariation with autonomic arousal and affective report. *Biological psychology* 52:95–111. [PubMed: 10699350]
- De Martino B, Fleming SM, Garrett N, Dolan RJ (2013) Confidence in value-based choice. *Nat Neurosci* 16:105–110. [PubMed: 23222911]
- Debener S, Ullsperger M, Siegel M, Engel AK (2006) Single-trial EEG–fMRI reveals the dynamics of cognitive function. *Trends in Cognitive Sciences* 10:558–563. [PubMed: 17074530]
- Delorme A, Makeig S (2004) EEGLAB: an open source toolbox for analysis of single-trial EEG dynamics including independent component analysis. *Journal of Neuroscience Methods* 134:9–21. [PubMed: 15102499]
- Etkin A, Buchel C, Gross JJ (2015) The neural bases of emotion regulation. *Nat Rev Neurosci* 16:693–700. [PubMed: 26481098]
- Etkin A, Egner T, Kalisch R (2011) Emotional processing in anterior cingulate and medial prefrontal cortex. *Trends in Cognitive Sciences* 15:85–93. [PubMed: 21167765]
- Fahrenfort JJ, Snijders TM, Heinen K, van Gaal S, Scholte HS, Lamme VAF (2012) Neuronal integration in visual cortex elevates face category tuning to conscious face perception. *Proceedings of the National Academy of Sciences* 109:21504–21509.
- Ferrari V, Codispoti M, Cardinale R, Bradley MM (2008) Directed and Motivated Attention during Processing of Natural Scenes. *Journal of Cognitive Neuroscience* 20:1753–1761. [PubMed: 18370595]
- Fischer Adrian G, Ullsperger M (2013) Real and Fictive Outcomes Are Processed Differently but Converge on a Common Adaptive Mechanism. *Neuron* 79:1243–1255. [PubMed: 24050408]

- Freedman DJ, Riesenhuber M, Poggio T, Miller EK (2001) Categorical Representation of Visual Stimuli in the Primate Prefrontal Cortex. *Science* 291:312–316. [PubMed: 11209083]
- Fuentemilla L, Marco-Pallarés J, Grau C (2006) Modulation of spectral power and of phase resetting of EEG contributes differentially to the generation of auditory event-related potentials. *Neuroimage* 30:909–916. [PubMed: 16376575]
- Garrison KA, Scheinost D, Worhunsky PD, Elwafi HM, Thornhill TA, Thompson E, Saron C, Desbordes G, Kober H, Hampson M (2013) Real-time fMRI links subjective experience with brain activity during focused attention. *Neuroimage* 81:110–118. [PubMed: 23684866]
- Hajcak G, Anderson BS, Arana A, Borckardt J, Takacs I, George MS, Nahas Z (2010) Dorsolateral prefrontal cortex stimulation modulates electrocortical measures of visual attention: evidence from direct bilateral epidural cortical stimulation in treatment-resistant mood disorder. *Neuroscience* 170:281–288. [PubMed: 20451585]
- Hajcak G, Dunning JP, Foti D (2009) Motivated and controlled attention to emotion: Time-course of the late positive potential. *Clinical Neurophysiology* 120:505–510. [PubMed: 19157974]
- Heinze HJ, Mangun GR, Burchert W, Hinrichs H, Scholz M, Munte TF, Gos A, Scherg M, Johannes S, Hundeshagen H, Gazzaniga MS, Hillyard SA (1994) Combined spatial and temporal imaging of brain activity during visual selective attention in humans. *Nature* 372:543–546. [PubMed: 7990926]
- Herry C, Bach DR, Esposito F, Di Salle F, Perrig WJ, Scheffler K, Luthi A, Seifritz E (2007) Processing of Temporal Unpredictability in Human and Animal Amygdala. *The Journal of Neuroscience* 27:5958–5966. [PubMed: 17537966]
- Hillyard SA, Squires KC, Bauer JW, Lindsay PH (1971) Evoked Potential Correlates of Auditory Signal Detection. *Science* 172:1357. [PubMed: 5580218]
- Hsu M, Bhatt M, Adolphs R, Tranel D, Camerer CF (2005) Neural Systems Responding to Degrees of Uncertainty in Human Decision-Making. *Science* 310:1680–1683. [PubMed: 16339445]
- Hu J, Cao Y, Blue PR, Zhou X (2014) Low social status decreases the neural salience of unfairness. *Frontiers in behavioral neuroscience* 8. [PubMed: 24478655]
- Huettel SA, Stowe CJ, Gordon EM, Warner BT, Platt ML (2006) Neural signatures of economic preferences for risk and ambiguity. *Neuron* 49:765–775. [PubMed: 16504951]
- Kelly SP, O’Connell RG (2013) Internal and External Influences on the Rate of Sensory Evidence Accumulation in the Human Brain. *The Journal of Neuroscience* 33:19434–19441. [PubMed: 24336710]
- Kelly SP, O’Connell RG (2015) The neural processes underlying perceptual decision making in humans: Recent progress and future directions. *Journal of Physiology-Paris* 109:27–37.
- Kennerley SW, Walton ME, Behrens TEJ, Buckley MJ, Rushworth MFS (2006) Optimal decision making and the anterior cingulate cortex. *Nat Neurosci* 9:940–947. [PubMed: 16783368]
- Kiani R, Corthell L, Shadlen Michael N (2014) Choice Certainty Is Informed by Both Evidence and Decision Time. *Neuron* 84:1329–1342. [PubMed: 25521381]
- Kolling N, Behrens TEJ, Mars RB, Rushworth MFS (2012) Neural Mechanisms of Foraging. *Science* 336:95. [PubMed: 22491854]
- Krain AL, Wilson AM, Arbuckle R, Castellanos FX, Milham MP (2006) Distinct neural mechanisms of risk and ambiguity: A meta-analysis of decision-making. *NeuroImage* 32:477–484. [PubMed: 16632383]
- Kutas M, McCarthy G, Donchin E (1977) Augmenting mental chronometry: the P300 as a measure of stimulus evaluation time. *Science* 197:792. [PubMed: 887923]
- Lebreton M, Abitbol R, Daunizeau J, Pessiglione M (2015) Automatic integration of confidence in the brain valuation signal. *Nat Neurosci* 18:1159–1167. [PubMed: 26192748]
- Leite J, Carvalho S, Galdo-Alvarez S, Alves J, Sampaio A, Gonçalves ÓF (2012) Affective picture modulation: Valence, arousal, attention allocation and motivational significance. *International Journal of Psychophysiology* 83:375–381. [PubMed: 22226675]
- Levy I, Snell J, Nelson AJ, Rustichini A, Glimcher PW (2010) Neural Representation of Subjective Value Under Risk and Ambiguity. *Journal of Neurophysiology* 103:1036–1047. [PubMed: 20032238]

- Lieberman MD, Eisenberger NI (2005) A pain, by any other name (rejection, exclusion, ostracism), still hurts the same: The role of dorsal anterior cingulate cortex in social and physical pain In: Social neuroscience: People thinking about people (Cacioppo JT. et al. eds) Cambridge, MA: MIT Press.
- Liu Y, Huang H, McGinnis-Deweese M, Keil A, Ding M (2012) Neural substrate of the late positive potential in emotional processing. *The Journal of Neuroscience* 32:14563–14572. [PubMed: 23077042]
- Lopez-Calderon J, Luck SJ (2014) ERPLAB: an open-source toolbox for the analysis of event-related potentials. *Frontiers in human neuroscience* 8. [PubMed: 24478674]
- Luck SJ (2014) An introduction to the event-related potential technique: MIT press.
- MacKinnon DP, Fairchild AJ, Fritz MS (2006) Mediation Analysis. *Annual Review of Psychology* 58:593–614.
- Moratti S, Saugar C, Strange BA (2011) Prefrontal-Occipitoparietal Coupling Underlies Late Latency Human Neuronal Responses to Emotion. *The Journal of Neuroscience* 31:17278–17286. [PubMed: 22114294]
- Murphy PR, Robertson IH, Harty S, O’Connell RG (2015) Neural evidence accumulation persists after choice to inform metacognitive judgments. *eLife* 4:e11946. [PubMed: 26687008]
- Nguyen VT, Cunnington R (2014) The superior temporal sulcus and the N170 during face processing: Single trial analysis of concurrent EEG–fMRI. *NeuroImage* 86:492–502. [PubMed: 24185024]
- Nomura M, Iidaka T, Kakehi K, Tsukiura T, Hasegawa T, Maeda Y, Matsue Y (2003) Frontal lobe networks for effective processing of ambiguously expressed emotions in humans. *Neuroscience Letters* 348:113–116. [PubMed: 12902031]
- Nunez PL, Srinivasan R (2006) *Electric fields of the brain: the neurophysics of EEG*: Oxford university press.
- O’Connell RG, Dockree PM, Kelly SP (2012) A supramodal accumulation-to-bound signal that determines perceptual decisions in humans. *Nat Neurosci* 15:1729–1735. [PubMed: 23103963]
- Pascual-Marqui RD, Michel CM, Lehmann D (1994) Low resolution electromagnetic tomography: a new method for localizing electrical activity in the brain. *International Journal of Psychophysiology* 18:49–65. [PubMed: 7876038]
- Pastor MC, Bradley MM, Löw A, Versace F, Moltó J, Lang PJ (2008) Affective picture perception: Emotion, context, and the late positive potential. *Brain Research* 1189:145–151. [PubMed: 18068150]
- Peng W, Hu L, Zhang Z, Hu Y (2012) Causality in the Association between P300 and Alpha Event-Related Desynchronization. *PLoS ONE* 7:e34163. [PubMed: 22511933]
- Penny W, Holmes A (2004) Random-effects analysis In: *Human brain function* (Frackowiak R et al. eds), pp 843–850 San Diego: Elsevier.
- Pfabigan DM, Seidel E-M, Sladky R, Hahn A, Paul K, Grahl A, Küblböck M, Kraus C, Hummer A, Kranz GS (2014) P300 amplitude variation is related to ventral striatum BOLD response during gain and loss anticipation: An EEG and fMRI experiment. *NeuroImage* 96:12–21. [PubMed: 24718288]
- Polich J (2007) Updating P300: An integrative theory of P3a and P3b. *Clinical Neurophysiology* 118:2128–2148. [PubMed: 17573239]
- Pouget A, Drugowitsch J, Kepecs A (2016) Confidence and certainty: distinct probabilistic quantities for different goals. *Nat Neurosci* 19:366–374. [PubMed: 26906503]
- Ritter W, Simson R, Vaughan HG Jr (1972) Association cortex potentials and reaction time in auditory discrimination. *Electroencephalography and Clinical Neurophysiology* 33:547–555. [PubMed: 4117332]
- Roy S, Roy C, Fortin I, Ethier-Majcher C, Belin P, Gosselin F (2007) A dynamic facial expression database. *Journal of Vision* 7:944–944.
- Rushworth MFS, Behrens TEJ (2008) Choice, uncertainty and value in prefrontal and cingulate cortex. *Nat Neurosci* 11:389–397. [PubMed: 18368045]
- Sabatinielli D, Lang PJ, Keil A, Bradley MM (2007) Emotional Perception: Correlation of Functional MRI and Event-Related Potentials. *Cerebral Cortex* 17:1085–1091. [PubMed: 16769742]

- Salomons TV, Johnstone T, Backonja M-M, Davidson RJ (2004) Perceived Controllability Modulates the Neural Response to Pain. *The Journal of Neuroscience* 24:7199–7203. [PubMed: 15306654]
- Scharmüller W, Leutgeb V, Schäfer A, Köchel A, Schienle A (2011) Source localization of late electrocortical positivity during symptom provocation in spider phobia: An sLORETA study. *Brain Research* 1397:10–18. [PubMed: 21600565]
- Scherg M (1990) Fundamentals of dipole source potential analysis In: *Auditory evoked magnetic fields and electric potentials*, vol. 6 (Grandori F et al. eds), pp 40–69 Basel: Karger.
- Schupp HT, Cuthbert BN, Bradley MM, Cacioppo JT, Ito T, Lang PJ (2000) Affective picture processing: the late positive potential is modulated by motivational relevance. *Psychophysiology* 37:257–261. [PubMed: 10731776]
- Shackman AJ, Salomons TV, Slagter HA, Fox AS, Winter JJ, Davidson RJ (2011) The integration of negative affect, pain and cognitive control in the cingulate cortex. *Nat Rev Neurosci* 12:154–167. [PubMed: 21331082]
- Shenhav A, Botvinick Matthew M, Cohen Jonathan D (2013) The Expected Value of Control: An Integrative Theory of Anterior Cingulate Cortex Function. *Neuron* 79:217–240. [PubMed: 23889930]
- Shenhav A, Straccia MA, Cohen JD, Botvinick MM (2014) Anterior cingulate engagement in a foraging context reflects choice difficulty, not foraging value. *Nat Neurosci* 17:1249–1254. [PubMed: 25064851]
- Sheth SA, Mian MK, Patel SR, Asaad WF, Williams ZM, Dougherty DD, Bush G, Eskandar EN (2012) Human dorsal anterior cingulate cortex neurons mediate ongoing behavioural adaptation. *Nature* 488:218–221. [PubMed: 22722841]
- Simmons A, Matthews SC, Paulus MP, Stein MB (2008) Intolerance of uncertainty correlates with insula activation during affective ambiguity. *Neuroscience Letters* 430:92–97. [PubMed: 18079060]
- Simmons A, Stein MB, Matthews SC, Feinstein JS, Paulus MP (2006) Affective ambiguity for a group recruits ventromedial prefrontal cortex. *Neuroimage* 29:655–661. [PubMed: 16125977]
- Sternberg S (1969) The discovery of processing stages: Extensions of Donders' method. *Acta Psychologica* 30:276–315.
- Terzer P, Kleinschmidt A (2007) A neural basis for inference in perceptual ambiguity. *Proceedings of the National Academy of Sciences* 104:323–328.
- Sutton S, Braren M, Zubin J, John E (1965a) Evoked-potential correlates of stimulus uncertainty. *Science* 150:1187–1188. [PubMed: 5852977]
- Sutton S, Braren M, Zubin J, John ER (1965b) Evoked-Potential Correlates of Stimulus Uncertainty. *Science* 150:1187–1188. [PubMed: 5852977]
- Tanner D, Morgan-Short K, Luck SJ (2015) How inappropriate high-pass filters can produce artifactual effects and incorrect conclusions in ERP studies of language and cognition. *Psychophysiology* 52:997–1009. [PubMed: 25903295]
- Wang S, Yu R, Tyszka JM, Zhen S, Kovach C, Sun S, Huang Y, Hurlmann R, Ross IB, Chung JM, Mamelak AN, Adolphs R, Rutishauser U (2017) The human amygdala parametrically encodes the intensity of specific facial emotions and their categorical ambiguity. *Nature Communications* 8:14821.
- Weinberg A, Ferri J, Hajcak G (2013) Interactions between Attention and Emotion: Insights from the Late Positive Potential In: *Handbook of cognition and emotion* (Robinson M et al. eds), pp 35–54 New York: Guilford Publications.
- Wiemer J, Pauli P (2016) Enhanced functional connectivity between sensorimotor and visual cortex predicts covariation bias in spider phobia. *Biological Psychology*.
- Willadsen-Jensen EC, Ito TA (2006) Ambiguity and the timecourse of racial perception. *Social Cognition* 24:580–606.
- Willenbockel V, Sadr J, Fiset D, Horne G, Gosselin F, Tanaka J (2010) Controlling low-level image properties: The SHINE toolbox. *Behavior Research Methods* 42:671–684. [PubMed: 20805589]
- Yoder KJ, Decety J (2014) Spatiotemporal neural dynamics of moral judgment: A high-density ERP study. *Neuropsychologia* 60:39–45. [PubMed: 24905282]

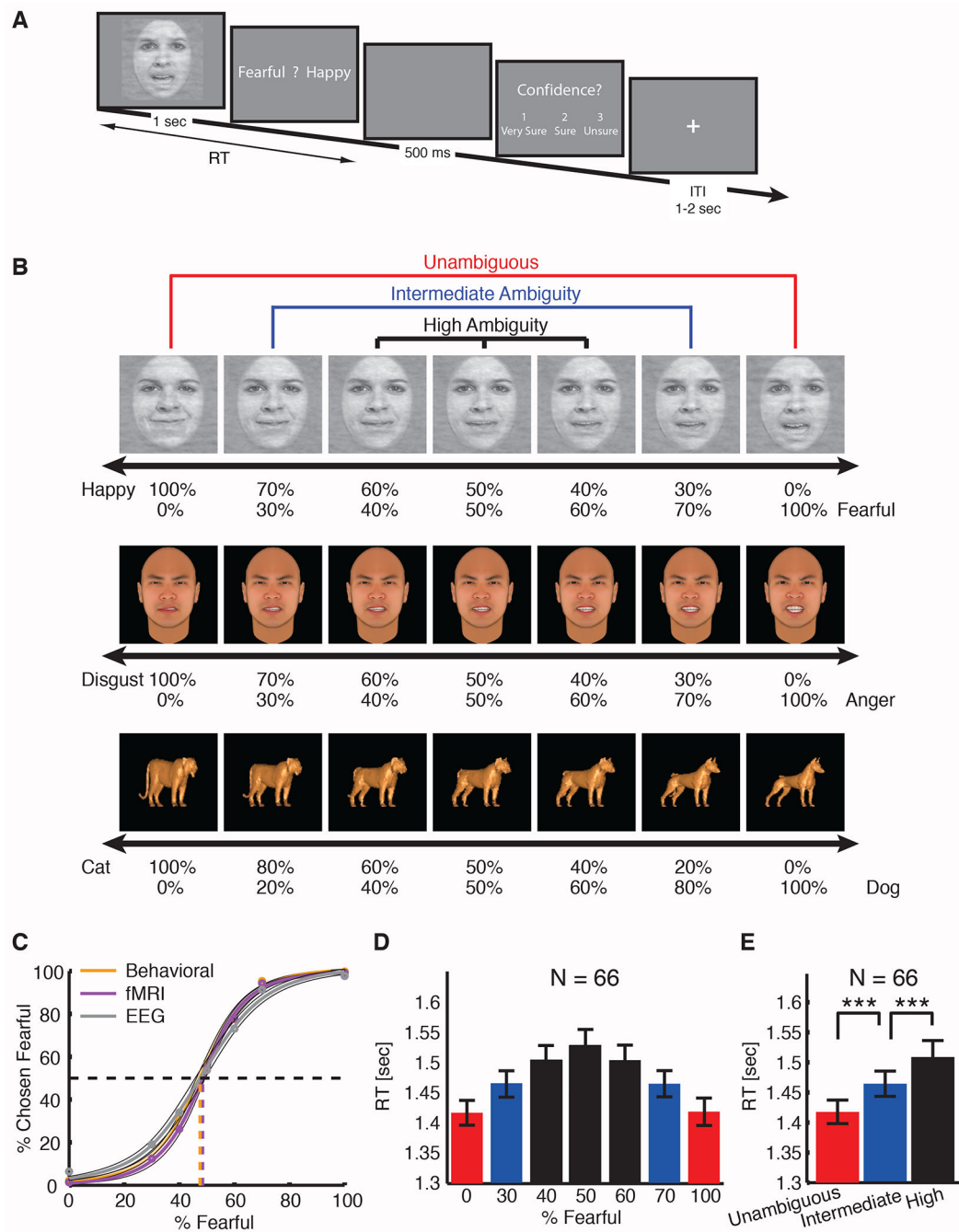
- Yoshida W, Ishii S (2006) Resolution of uncertainty in prefrontal cortex. *Neuron* 50:781–789.
[PubMed: 16731515]
- Young AW, Rowland D, Calder AJ, Etcoff NL, Seth A, Perrett DI (1997) Facial expression megamix:
Tests of dimensional and category accounts of emotion recognition. *Cognition* 63:271–313.
[PubMed: 9265872]

Author Manuscript

Author Manuscript

Author Manuscript

Author Manuscript

**Fig. 1.**

Task, sample stimuli, and behavioral results. **(A)** Task. A face was presented for 1 second followed by a question asking subjects to identify the facial emotion (fearful or happy). For behavioral subjects, after a blank screen of 500ms, they were then asked to indicate their confidence in their decision ('1' for 'very sure', '2' for 'sure' or '3' for 'unsure'). Faces are not shown to scale. **(B)** Sample stimuli. Top: sample stimuli of one female identity ranging from 100% happy/0% fearful to 0% happy/100% fearful. Middle: sample stimuli of one male identity ranging from 100% disgust/0% anger to 0% disgust/100% anger. Bottom:

sample stimuli of an animal ranging from 100% cat/0% dog to 0% cat/100% dog. Three ambiguity levels (unambiguous, intermediate, and high) are grouped as shown above the stimuli. **(C-E)** Behavioral results. **(C)** Group average of psychometric curves showing the proportion of trials judged as fearful as a function of morph levels (ranging from 0% fearful (100% happy; on the left) to 100% fearful (0% happy; on the right)). Shaded area denotes \pm SEM across subjects. Emotion judgment index (EJI) was defined as the point on x-axis where the percentage of judging fearful (y-axis) reaches 50% (dotted lines). **(D)** The reaction time (RT; relative to stimulus onset) for the fear/happy decision, which can be considered as an implicit measure of confidence. Error bars denote one SEM across subjects. **(E)** RT when grouping the 7 morph levels into 3 ambiguity levels. Subjects judged facial emotions faster for unambiguous faces but slower for more ambiguous faces. Paired t-test between adjacent levels of ambiguity: ***: $P < 0.001$.

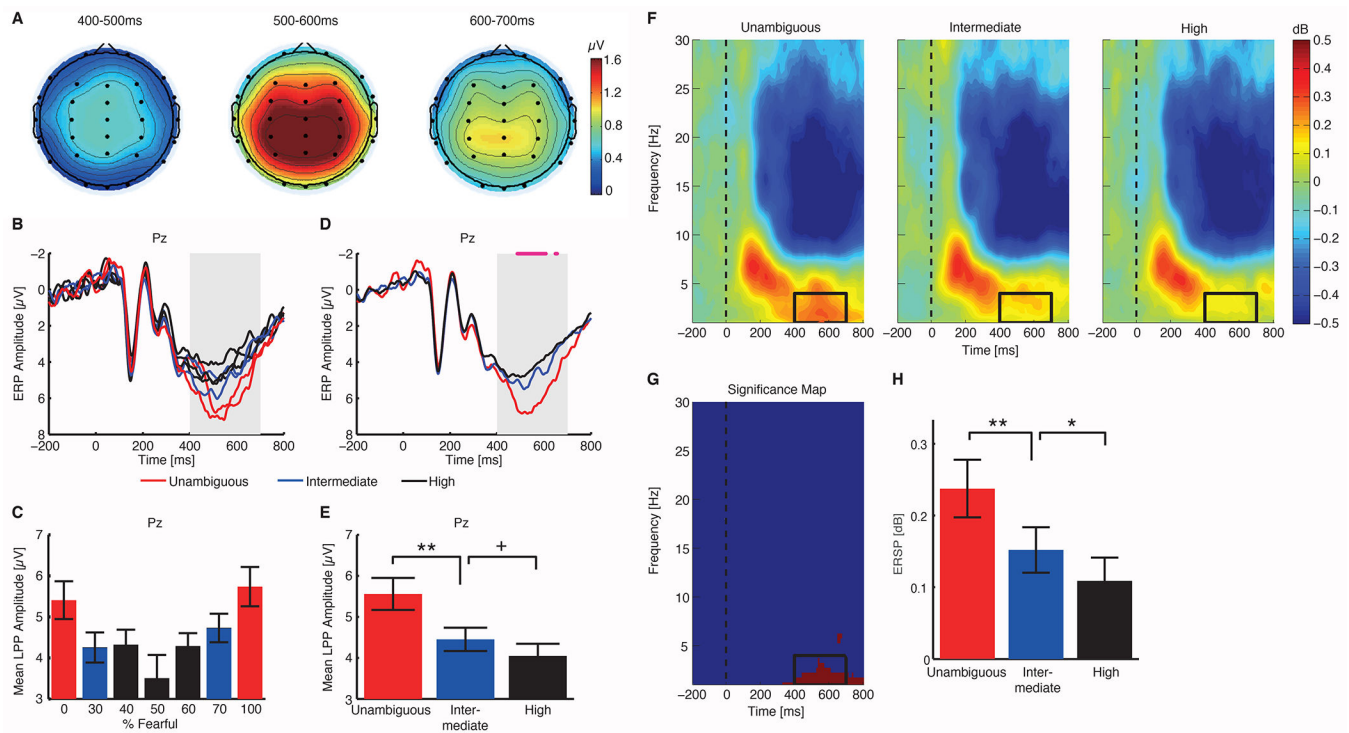


Fig. 2.

ERP results. **(A)** Topography during the LPP interval (400-700ms after stimulus onset) for unambiguous minus the most ambiguous faces. **(B, D)** ERP at the electrode Pz differentiated ambiguity levels. Gray shaded area denotes the LPP interval. The top magenta bars in **(D)** illustrate the points with significant difference across three ambiguity levels (one-way repeated-measure ANOVA, $P < 0.05$, corrected by FDR for $Q < 0.05$ (Benjamini and Hochberg, 1995)). **(C, E)** Mean LPP amplitude. LPP amplitudes were averaged across the entire interval (shaded area in **(B, D)**). U-shaped LPP amplitudes with respect to morph levels **(C)** (one-way repeated-measure ANOVA of morph levels: $F(6,132) = 5.25$, $P = 7.06 \times 10^{-5}$, $\eta_p^2 = 0.19$) showed a parametric modulation of LPP amplitudes by facial ambiguity (one-way repeated-measure ANOVA of ambiguity levels: $F(2,44) = 11.1$, $P = 1.27 \times 10^{-4}$, $\eta_p^2 = 0.34$; unambiguous: $5.56 \pm 1.87 \mu\text{V}$ (mean \pm SD); intermediate: $4.45 \pm 1.36 \mu\text{V}$; high: $4.05 \pm 1.42 \mu\text{V}$). Error bars denote one SEM across subjects. Paired t-test between adjacent levels of ambiguity: **: $P < 0.01$, and +: $P < 0.1$. **(F)** Time-frequency plots depicting the power of oscillations for each ambiguity level. Black dashed line denotes stimulus onset (Time=0). Unambiguous stimuli had a significantly higher power in the delta frequency band (1-4Hz) in the LPP time window (black rectangle) compared to more ambiguous stimuli. **(G)** Significance map. Red: time and frequency that show significant difference (one-way repeated-measure ANOVA of ambiguity levels, $P < 0.05$, FDR corrected). **(H)** Mean power of the delta frequency band between 400 to 700ms after stimulus onset. Error bars denote one SEM across subjects. Asterisk indicates a significant difference between conditions. *: $P < 0.05$, and **: $P < 0.01$.

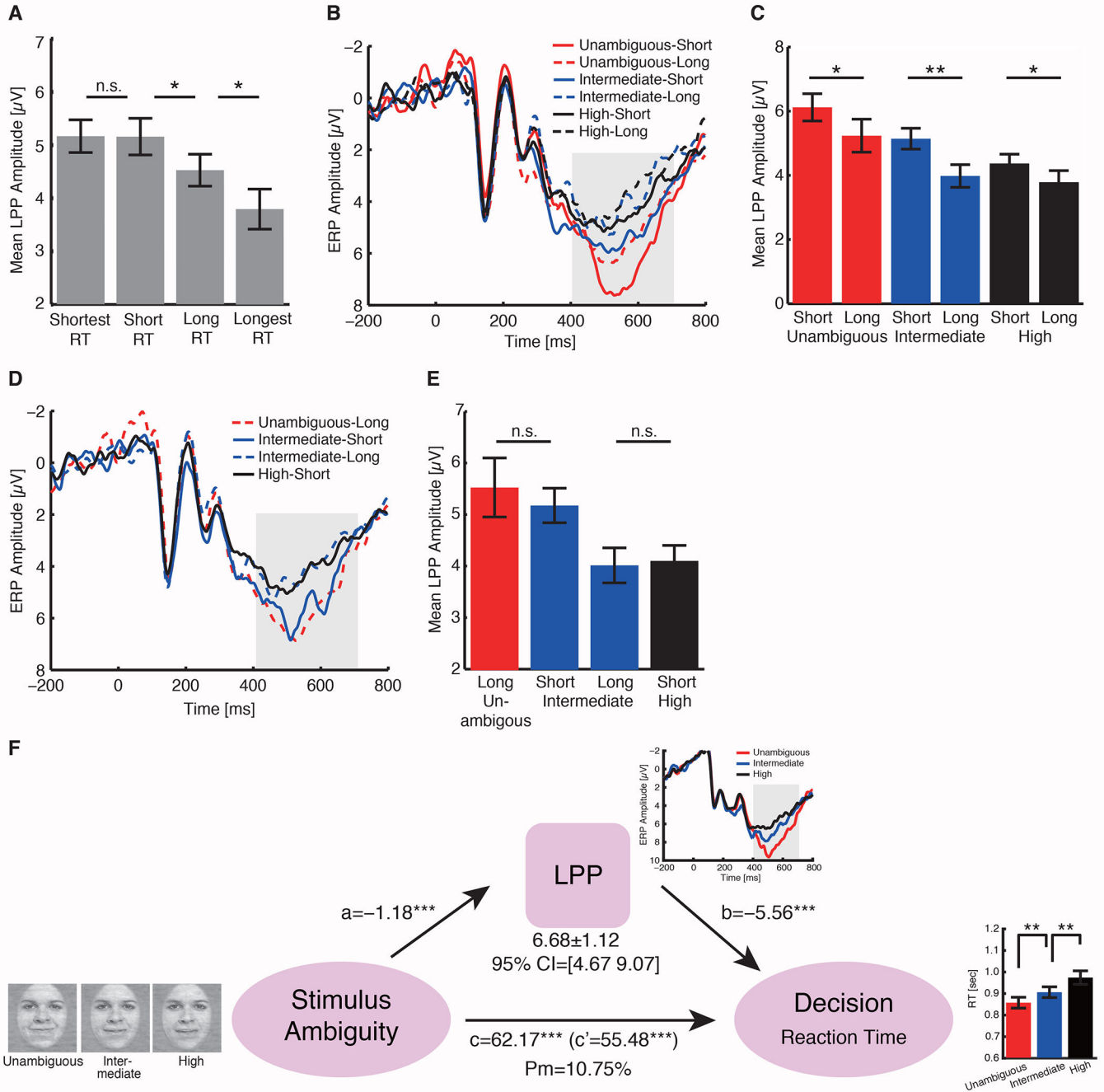


Fig. 3. The LPP is associated with behavioral judgment about ambiguity. **(A)** Trials with shorter RT had higher LPP amplitudes ($F(3,66)=7.48, P=2.19 \times 10^{-4}, \eta_p^2=0.25$). The LPP was sorted into 4 groups according to RT for each subject (one-way repeated-measure ANOVA of RT levels confirmed their difference: $F(3,66)=1341, P<10^{-20}, \eta_p^2=0.98$). Error bars denote one SEM across subjects. Asterisk indicates a significant difference between adjacent conditions using paired two-tailed t-test. *: $P<0.05$. n.s.: not significant. **(B, D)** ERP sorted according to ambiguity levels (color coding) and RT lengths (line type; solid: short, dashed: long). **(B)**

Higher LPP amplitudes were not only associated with lower ambiguity, but also associated with shorter RTs within each ambiguity level. **(D)** LPPs from trials with similar RTs were similar even for different ambiguity levels. Gray shaded area denotes the LPP interval. **(C, E)** Mean LPP amplitude for each condition shown in **(B, D)**, respectively. LPP amplitudes were averaged across the entire interval (shaded area in **(B, D)**). **(C)** Within each ambiguity level, higher LPP amplitudes were always associated with shorter RTs regardless of the same stimulus (paired two-tailed t-test; unambiguous: $t(22)=2.13$, $P=0.044$, $d=0.44$; intermediate: $t(22)=3.21$, $P=0.004$, $d=0.67$; high: $t(22)=2.10$, $P=0.047$, $d=0.44$). A two-way repeated-measure ANOVA on the mean LPP amplitude (ambiguity level (unambiguous vs. intermediate vs. high) X RT group (long vs. short)) revealed significant main effects for both ambiguity level ($F(2,44)=11.2$, $P=0.001$, $\eta_p^2=0.34$) and RT group ($F(1,44)=15.1$, $P=0.001$, $\eta_p^2=0.41$), but no significant interaction between ambiguity level and RT group ($F(2,44)=0.71$, $P=0.50$, $\eta_p^2=0.03$). **(E)** Between adjacent ambiguity levels, similar LPP amplitudes were found for similar RTs regardless of different ambiguity levels (unambiguous vs. intermediate: $t(22)=0.78$, $P=0.45$, $d=0.16$ for LPP and $t(22)=-1.49$, $P=0.15$, $d=-0.32$ for RT; intermediate vs. high: $t(22)=-0.32$, $P=0.75$, $d=-0.07$ for LPP and $t(22)=-0.26$, $P=0.80$, $d=-0.06$ for RT). Error bars denote one SEM across subjects. Asterisk indicates a significant difference between conditions using paired two-tailed t-test. *: $P<0.05$ and **: $P<0.01$. n.s.: not significant. **(F)** Statistical mediation analysis. Path diagram depicts the relationships between nodes in a mediation model that tested whether the LPP amplitude mediated the relationship between stimulus ambiguity and RT. Lines are labeled with path coefficients. Stimulus ambiguity (predictor, left) predicted the LPP amplitude (mediator, middle), which in turn predicted RT (outcome, right) controlling for stimulus ambiguity. The upper middle coefficient indicates the formal mediation effect (mean \pm SEM). The significant direct path between stimulus ambiguity and RT, calculated controlling for the mediator, indicates partial mediation: the LPP amplitude did not explain all of the shared variance between stimulus ambiguity and RT. ***: $P<0.001$, 5000 bootstraps.

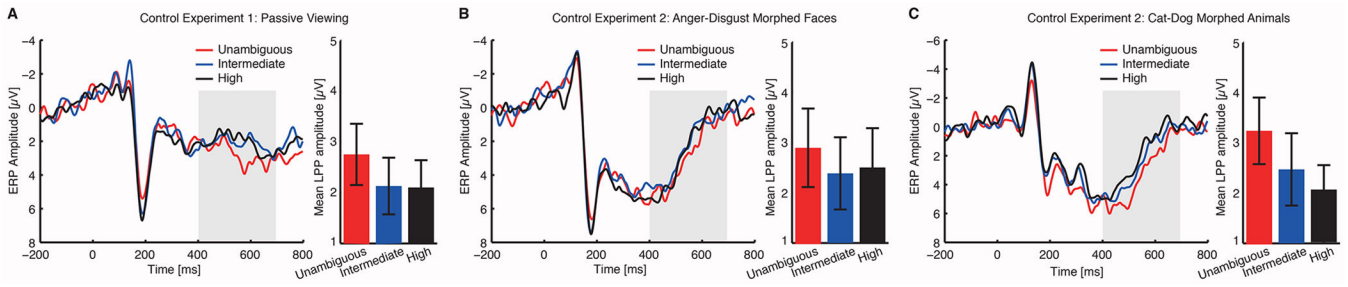


Fig. 4. Control experiments show a direct relationship between the LPP and behavioral response to ambiguity. **(A)** The LPP was abolished when subjects freely viewed the faces without judging emotions (one-way repeated-measure ANOVA of ambiguity levels; mean amplitude: $F(2,28)=0.63$, $P=0.54$, $\eta_p^2=0.04$; peak amplitude: $F(2,28)=0.97$, $P=0.39$, $\eta_p^2=0.07$; peak latency: $F(2,28)=0.29$, $P=0.75$, $\eta_p^2=0.02$). **(B, C)** The LPP was abolished when subjects judged whether the stimulus was a human face or an animal, an unambiguous aspect of the stimuli. **(B)** Anger-disgust morphed faces (mean amplitude: $F(2,28)=0.45$, $P=0.64$, $\eta_p^2=0.03$; peak amplitude: $F(2,28)=0.35$, $P=0.71$, $\eta_p^2=0.02$). **(C)** Cat-dog morphed animals (mean amplitude: $F(2,28)=2.52$, $P=0.098$, $\eta_p^2=0.15$; peak amplitude: $F(2,28)=2.26$, $P=0.12$, $\eta_p^2=0.14$). ERP is shown on the left and the mean ERP amplitude in the LPP interval is shown on the right. Conventions as Fig. 3.

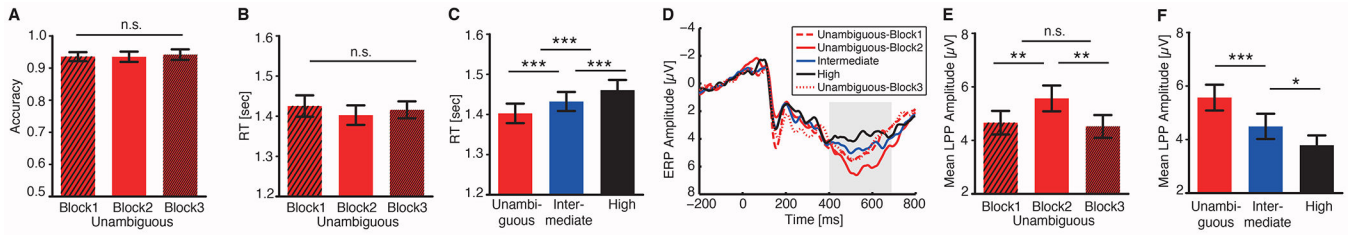


Fig. 5.

Context modulation of the LPP. **(A)** Accuracy of judging unambiguous faces did not differ between blocks (first block: $93.6 \pm 7.91\%$ (mean \pm SD); second block: $93.5 \pm 9.03\%$; third block: $94.2 \pm 9.38\%$; one-way repeated-measure ANOVA: $F(2,62)=0.19$, $P=0.81$, $\eta_p^2=0.006$). **(B)** RT of unambiguous faces did not differ between blocks (first block: 1.425 ± 0.15 s; second block: 1.402 ± 0.14 s; third block: 1.415 ± 0.12 s; $F(2,62)=0.88$, $P=0.42$, $\eta_p^2=0.028$). **(C)** RT differed significantly as a function of ambiguity levels in the second block (unambiguous: 1.402 ± 0.14 s; intermediate: 1.432 ± 0.13 s; high: 1.460 ± 0.14 s; $F(2,62)=25.8$, $P=6.97 \times 10^{-9}$, $\eta_p^2=0.45$). **(D)** The LPP was not only modulated by ambiguity levels, but also by the context of ambiguous stimuli. **(E)** Mean LPP amplitude for unambiguous faces across blocks (first: $4.66 \pm 2.48 \mu\text{V}$; second: $5.57 \pm 2.73 \mu\text{V}$; third: $4.52 \pm 2.40 \mu\text{V}$; $F(2,62)=5.80$, $P=0.005$, $\eta_p^2=0.158$). LPP amplitudes were averaged across the entire interval (shaded area). **(F)** Mean LPP amplitude for faces with different levels of ambiguity in the second block ($F(2,62)=21.27$, $P=9.22 \times 10^{-8}$, $\eta_p^2=0.407$). Error bars denote one SEM across subjects. Asterisk indicates a significant difference between conditions. *: $P < 0.05$, **: $P < 0.01$, and ***: $P < 0.001$. n.s.: not significant.

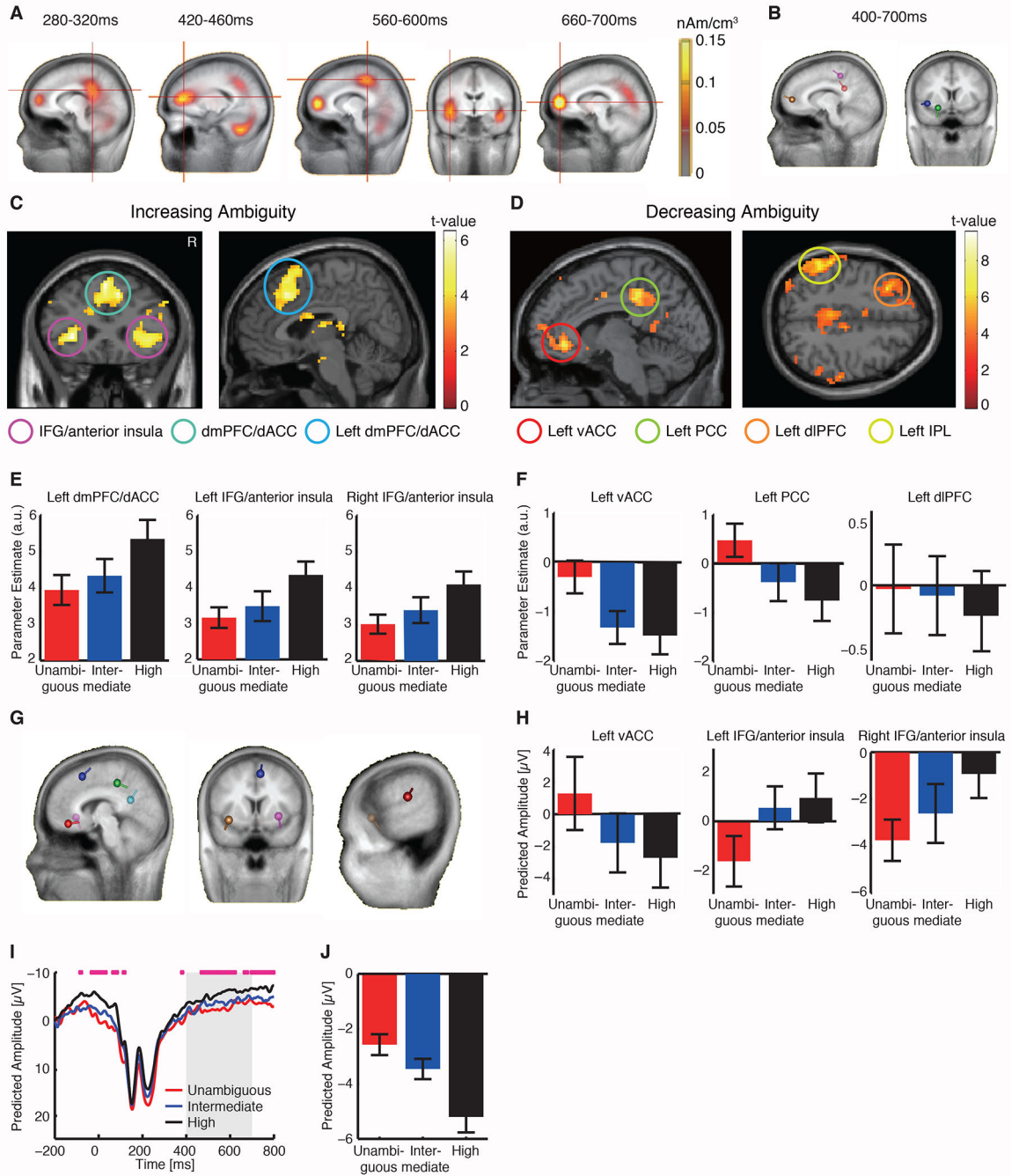


Fig. 6. Source localization and fMRI results. **(A, B)** Source localization of the LPP. Mean differential ERPs (unambiguous minus high ambiguity) were used to obtain the sources. Source locations are in standard Talairach space. **(A)** Sources estimated using a distributed model. The locations and intensities (color coding) of the regional sources are shown for a series of 40ms time intervals around the LPP time window (280-320ms, 420-460ms, 560-600ms, and 660-700ms). **(B)** Sources estimated using a discrete model. Five dipoles (4 fixed and 1 free) were fitted for the time interval of 400 to 700ms after stimulus onset. **(C)**

Increasing ambiguity was correlated with increasing BOLD activity in the bilateral IFG/ anterior insula and dmPFC/dACC. The generated statistical parametric map was superimposed on anatomical sections of the standardized MNI T1-weighted brain template. Images are in neurological format with subject left on image left. R: right. **(D)** Decreasing ambiguity was correlated with increasing BOLD activity in the left vACC, PCC, dlPFC, IPL, and right postcentral gyrus. **(E, F)** Parameter estimate (beta values) of the general linear model (GLM) for each ambiguity level (average of all activated voxels around the peak). Error bars denote one SEM across subjects. **(G)** Dipoles used to predict source waveforms. Dipole locations were selected as the peaks of the activated regions identified by fMRI: bilateral IFG, left dmPFC, left vACC, left PCC, right postcentral gyrus, and a free dipole. **(H)** Predicted source amplitudes in the LPP interval differentiated ambiguity levels and were consistent with the LPP and fMRI results (one-way repeated-measure ANOVA of ambiguity levels; left vACC: $F(2,44)=5.51$, $P=0.007$, $\eta_p^2=0.20$; left IFG/insula: $F(2,44)=3.53$, $P=0.038$, $\eta_p^2=0.14$; right IFG/insula: $F(2,44)=3.30$, $P=0.046$, $\eta_p^2=0.13$). Error bars denote one SEM across subjects. **(I)** Predicted source waveforms using all dipoles (bilateral IFG, left dmPFC, left vACC, left PCC, right postcentral gyrus, and a free dipole). Conventions as Fig. 2D. **(J)** Mean source amplitudes in the LPP interval. Error bars denote one SEM across subjects.